Journal of Materials Chemistry A

ROYAL SOCIETY OF CHEMISTRY

REVIEW

View Article Online
View Journal | View Issue

Cite this: J. Mater. Chem. A, 2023, 11, 9216

Advances in sensing mechanisms and micro/nanostructured sensing layers for surface acoustic wave-based gas sensors

Xue Li,[a] Wenfeng Sun,[a] Wei Fu,[a] Haifeng Lv,[a] Xiaotao Zu,*[a] Yuanjun Guo,*[a] Des Gibson[b] and Yong-Qing Fu*[c]

Received 29th December 2022
Accepted 7th March 2023

DOI: 10.1039/d2ta10014b

rsc.li/materials-a

Surface acoustic wave (SAW) technology has been extensively used in communications and sensing applications. For SAW based gas sensing applications, the sensitive material or sensing layer which is coated onto the SAW sensor is vital for its sensitivity, selectivity, limit of detection, and repeatability, as changes of sensing signals (including frequency, amplitude, and phase angle) are strongly linked to variations of mass loading, electrical conductivity and elastic modulus (or elastic loading) of this sensing layer. There have been rapid developments in this field recently but great challenges still remain in the choices of suitable sensing materials, structures and mechanisms of these sensing layers. This paper reviews recent advances of micro- and nanostructured sensing materials and their selection, their sensing mechanisms and designs towards enhancing the gas sensing performance of SAW devices. We first discuss different sensing mechanisms based on SAW principles, along with the key sensing influencing parameters. We then highlight and categorize recently reported gas sensing materials into semiconductor metal oxides, carbon-based materials and polymers. We further focus the discussion on the relationships among the micro/nanostructures, compositions, and structure-sensing performance of the SAW based sensors. Finally, we highlight key challenges and potential solutions as well as future directions of sensing materials for SAW based gas sensors.

1. Introduction

With the rapid development of economics worldwide, there are great concerns about environmental issues, public safety, and human health conditions, as various hazardous gases and numerous volatile organic compounds (VOCs) are released into the atmosphere, and pose great threats to cause severe diseases, damage of the living environment, and potential fire/explosions.[1–4] For example, hydrogen sulfide (H_2S) is colorless but harmful and toxic, and often causes adverse effects on people, even at a low concentration of 2 parts-per-million (ppm). It could be lethal if there is an exposure to H_2S up to 100 ppm.[5,6] Ammonia (NH_3) is another toxic gas which is commonly released by the combustion of the chemicals in industrial processes. Excessive NH_3 is pernicious to animals and plants.[7–9] Hydrogen (H_2) has also commonly been used in industry but is very dangerous and explosive.[10,11] Therefore, there are huge demands for rapid and accurate detection of these gases.

Currently, many types of sensors have been explored to detect various gases, such as impedance gas sensors, electrocatalytic gas sensors and optical gas sensors. Many impedance gas sensors are based on resistance or capacitance changes of semiconductors (such as conducting oxides) in the form of either thick films, porous pellets, or thin films. Nevertheless, they have many drawbacks such as slow recovery characteristics and poor sensitivity, especially at room temperature or low operating temperatures.[13] The principle of electrocatalytic gas sensors is the use of catalytic materials as the sensing layer to monitor changes of carrier concentrations, mainly due to the variations of the concentration of the measured gas in the test environment. However, the disadvantage of this type of gas sensor is its limited sensitivity and accuracy. An optical gas sensor is based on the principle that when the sensitive layer of the sensor adsorbs the gas molecules, the optical absorption spectrum of the sensor is changed which is associated with the type and concentration of the gas. However, the test equipment of this sensor is often bulky and expensive. Therefore, significant attention has been paid to enhance the sensitivity and selectivity of gas sensors, recovery characteristics, and/or wireless passive capabilities.

Acoustic wave based sensors, especially surface acoustic wave (SAW) sensors, are often used to detect various physical and chemical parameters such as temperature, pressure, mass

[a]School of Physics, University of Electronic Science and Technology of China, Chengdu, 610054, P. R. China. E-mail: guoyuanjun@uestc.edu.cn; xtzu@uestc.edu.cn
[b]Institute of Thin Films, Sensors and Imaging, University of the West of Scotland, Scottish Universities Physics Alliance, Paisley PA1 2BE, UK
[c]Faculty of Engineering and Environment, University of Northumbria, Newcastle upon Tyne, NE1 8ST, UK. E-mail: richard.fu@northumbria.ac.uk

percentage of solution, electric field, ion concentration, gas flow, and gas and vapor concentration.[14–17] They generally have high sensitivity, high selectivity and good stability. The first generation acoustic wave based resonators were developed in the nineteen sixties.[18] Later, ultra-high frequency SAW resonators up to GHz devices have been developed.[19,20] These SAW sensors have found wide applications in RF filters or couplers, and other types of electronic devices,[15,20–22] wireless communication tools, and smart miniaturized sensors.[23] By integrating with sensing layer materials, they show remarkably high sensitivity, small size, and fast response speed. The ability to integrate with different receptors or sensing layer materials are the distinct characteristics of SAW devices.[24–26] These features make them highly suitable for detecting a variety of gases such as VOCs,[27] toxic gases,[28] chemical warfare agents,[29] explosive gases[30] and bio-analytes.[31] With the continuously increasing demands, SAW devices are becoming widely used in the detection of toxic and harmful gases.

To date, different nanostructured sensing materials such as supramolecular coatings,[15,32,33] semiconductor metal oxides,[34–36] carbon-based materials,[37] self-assembled monolayers,[38] and polymers[39,40] have been synthesized and coated on a SAW device to detect various gases. Among them, semiconductor metal oxides, carbon-based materials, and polymers (Fig. 1) are the most commonly reported ones. Semiconductor metal oxides have high carrier concentrations and good chemical and thermal stabilities.[34,35] Carbon-based materials have many potentially good characteristics such as high sensitivity, structural diversity, good conductivity and low cost.[37,41] Polymer based materials show potentially excellent electromagnetic and microwave absorption performance, good electrochemical performance, high conductivity, good environmental stability, easy availability of raw materials and other characteristics making them a potential material to be applied in practice.[12,42]

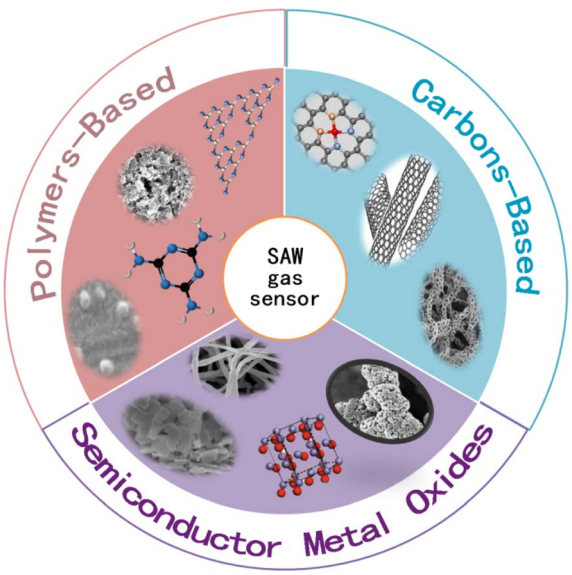

Fig. 1 Schematic diagram of various sensing material nanostructures used for SAW gas sensors.

Generally, an ideal sensing material deposited on SAW device should have the features of high efficiency, good stability, and excellent sensing performance under variable environmental conditions. However, in reality many sensing materials have issues of low sensitivity, poor long-term stability, or poor environmental intolerance. Therefore, exploring/designing new sensing materials and their sensing mechanisms for a targeted gas are urgently needed to improve the sensing efficiency of the SAW sensors. So far, there are not many review papers which focus on the sensing layer materials of SAW devices and the influences of these materials' characteristics on the sensing performance. A few of them are focused more on applications of wireless sensor networks in precision agriculture,[43] or basic principles and physical applications of SAW gas sensors,[44–46] and/or the applications of biosensing and microfluidic integration into the SAW sensor.[47,48] Moreover, with the continuous improvement and development of SAW gas sensor devices, enormous progress has been made recently in the design and preparation of significantly improved or new generation sensing layer materials. Therefore, this paper aims to review the intrinsic relationships among sensing materials (or the sensing layer), their characteristic designs of micro/nanostructures, and SAW gas sensing performances, shedding light on the rational design and synthesis of advanced gas sensing materials.

In this review, we firstly discussed the basic sensing mechanisms of SAW gas sensors, along with the key sensing parameters. Recent advances of gas sensing materials are then highlighted and the gas sensing materials are categorized into semiconductor metal oxide nanostructures, carbon-based materials and polymers from the aspects of microstructures, composition, and structure-sensing performance relationships. Finally, we highlight current challenges along with solutions and potential trends of sensing materials for SAW gas sensors.

2. Fundamentals of SAW gas sensing principles and mechanisms

SAW technology is attractive for the sensor industry because it conforms to the requirement of system miniaturization, digitization, intelligence, integration and high precision. SAW gas sensors commonly consist of a SAW device (such as those based on quartz, $LiNbO_3$ or thin films), sensitive adsorption materials and an external circuit.[1,14,15,17,19,26,35] To improve the sensor performance, a clear understanding of the sensing mechanisms and specifications is necessary.

2.1 Mechanisms of SAW based gas sensing

If a piezoelectric substrate is excited by the electric field, surface vibrations will be generated due to the piezoelectric effects. The vibration of the surrounding dielectric atoms or particles gives rise to the mechanical waves.[14,17,49] The commonly used piezoelectric substrate materials to generate SAWs include bulk substrates of quartz, $LiNbO_3$ and $LiTaO_3$, $PbZr_xTi_{(1-x)}O_3$ (PZT), or the films of AlN, ZnO, and GaN.[35,50–52] SAWs are mechanical waves rather than electromagnetic waves, and their propagation

speeds are much lower than those of electromagnetic waves (*e.g.*, speed of light), and they propagate along the surface of the material.[15,53] The most common wave modes are Rayleigh wave, Lamb wave, Love wave, and shear-horizontal wave.[54]

Acoustic waves are commonly generated on SAW devices by using periodic comb-shaped electrodes, called interdigital transducers (IDTs), which are a group of thin metal strips periodically arranged on the surface of a piezoelectric substrate and fabricated using the conventional photolithographic method.[55,56] These electrodes are generally made of metals such as Au/Cr, Al, or transparent conducting oxides (such as ITO and AZO).[56,57] IDTs are mainly used to excite and receive SAW signals. Different weighting methods of IDTs can improve the propagation direction and frequency characteristics of the SAW device, and also reduce the crosstalk among different SAW channels. Therefore, a few parameters should be paid attention when designing IDTs to improve the intrinsic properties of SAW devices. The first one is the center frequency of IDTs, which is determined by finger width and finger space as shown in Fig. 2a and b, and usually a higher center frequency leads to a better detection sensitivity. The second one is the bandwidth of the IDT, which depends on the interdigital logarithm and determines the signal generation and strength. It is worth mentioning that more the interdigital logarithms, stronger the excited SAWs. The third one is the geometrical shape of the IDT, which directly reflects the impulse responses of the excited SAWs. The output signal is a function of frequency changes in a sine function. Therefore, IDTs play an important role in the performance of acoustic surface devices.

There are two common designs of SAW devices, *i.e.*, delay line type (DL type) and resonator type (R type). The former one is shown in Fig. 2a, in which the SAWs are generated from one of the IDT1s, and then propagate along a delay line region to the opposite IDT2. In the R type one shown in Fig. 2b, the sensing layer is set in the middle, with two IDTs and reflectors at both ends, and the wave is reflected by metal strips or grooves in the wave propagation path.[58] The key working mechanism of the DL type-based SAW devices can be explained as follows. When the sensor receives the sinusoidal excitation signal through the antenna and transmits it to the IDTs, the SAW propagates on the piezoelectric substrate and reaches the reflection grid after a period of delay. The reflection grating reflects part of the sound wave, which is converted into a sinusoidal excitation signal through the IDT based on the piezoelectric effect, thereby realizing electro-acoustic conversion.[59] Due to the changes of properties at the delay line region (such as mechanical, physical or chemical properties), the frequency or phase angles of the waves will be changed, which can be used to predict the changes of sensing parameters.

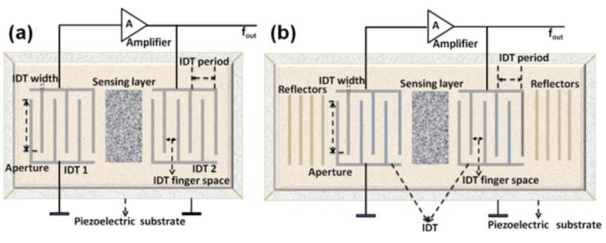

Fig. 2 (a) Delay line type of SAW sensor devices. (b) Resonator type of SAW sensor devices.

SAW-based gas detection is mostly based on chemical or physical adsorption, through the property changes of the sensing film on the SAW device surface.[60] The sensor material coated on the quartz device adsorbs gas molecules from the surrounding atmosphere, and then the propagation velocities of surface waves are changed. Among all the effects, the most significant one is that adsorption of gas molecules results in the changes of mass loading, which leads to the shift of the resonant frequencies.[61] By comparing the degrees of frequency shifts or phase angle changes, we can detect the gas molecule absorption using the SAW sensor. Eqn (1) reveals the relationship between the frequency shift and mass loading change:[61,62]

$$\Delta f = -\frac{k\Delta m {f_0}^2}{A} \quad (1)$$

where Δf represents the frequency shift caused by mass change, f_0 is the central frequency of SAW resonators, K is the material constant, Δm is the mass loading and A is the sensing area.

Elastic loading is associated with the changes of the surface viscosity of the sensing layer in the gas atmosphere, resulting in the change of the wave speed. It is another parameter that causes the frequency shift/response, which can be described using the following equation:[62,63]

$$\Delta f = C_e h {f_0}^2 \times \left(\left(\frac{4\mu}{{v_0}^2}\right) \times \left(\frac{\mu+\lambda}{\mu+2\lambda}\right)\right) \quad (2)$$

where C_e is the sensitivity coefficient for elasticity, h represents the thickness of the sensing material film, f_0 represents the fundamental resonance frequency, V_0 is the original SAW propagation speed (3158 m s^{-1}), and λ and μ are the bulk and shear modulus of elasticity, respectively.

Electric loading is related to the changes in the electrical characteristics (such as conductivity and permittivity) of the sensitive layer after adsorbing the gas, which causes the center frequency of the resonator to shift. It can be expressed by the following equation:[64]

$$\frac{\Delta V}{V_0} = -\frac{k^2}{2} \times \left(\frac{1}{1+\left(\frac{V_0 C_s}{\sigma_s}\right)^2}\right) \quad (3)$$

where k^2 is the electromechanical coupling coefficient, V_0 is the original SAW propagation speed (3158 m s^{-1}), σ_s is the initial conductivity of the sensing film, and C_s represents the capacitance per unit length of the device.

Mass loading, elastic loading and electric effect could have totally different influences on the frequency changes (*i.e.*, increase or decrease), as revealed by eqn (1)–(3). These three effects affect the sensing response characteristics of SAW gas sensors. We should address the issue that the mass loading and other loadings show opposite changes in the frequency values of the SAW sensor after the target vapors and molecules are adsorbed onto the SAW device.[34,62,64]

2.2 Performance indicators of SAW gas sensors

To evaluate the performance of a SAW gas sensor, several key indicators need to be considered, *e.g.*, selectivity, sensitivity and stability.

Selectivity refers to the ability of a SAW gas sensor to sense a specific gas among various other types of gases. It is one of the basic requirements of a sensing material, and is commonly determined by comparing the signal changes which are generated by the absorption of a certain concentration of tested gas and those of interfering gases.[65] For different types of gases, different sensing layers might be needed for selective detection, and sensing layers with excellent selectivity will absorb the specific gas to be measured among a mixture of gases. Therefore, the selectivity for a specific gas is the most basic requirement of a sensor material, and it is also the ultimate goal of the SAW gas sensor.

Sensitivity refers to the minimum concentration of the target gas that can be detected. It is also usually defined as the ratio of the relative frequency shift to the concentration ($\Delta f/\Delta c$, where Δf is the shift of the vibration frequency and Δc is the change in the concentration of the detected gas).[65] In the experimental process, there are many factors that can affect the sensitivity of the SAW sensor, such as temperature, humidity, surface area and conductivity of the sensing material. For example, Fan *et al.*[66,67] discussed the effect of conductivity on SAW sensor sensitivity and reported that changes in mass loading and conductivity shifted the central frequency of the sensor in opposite directions. If the conductivity of the sensitive layer is increased due to the absorption of the gases, the combined effects will cause increase of the sensitivity. Through simulation, they found that the sensitivity of the SAW gas sensors can be improved by optimizing the operating frequencies, structural parameters and properties of the multilayered materials in the sensors.[68]

Stability means that the sensor can continue to work stably without attenuation under various conditions such as high temperature, high pressure and corrosive environment.[65,69] Whether designed for commercial market applications or for experimental testing, SAW gas sensors must guarantee the stability of their sensing performance. They should display stable and repeatable signals over a period of time or after many cycles of testing. Here the stability includes both chemical and physical ones, such as the chemical's structure and composition, and the thermal stability and functional (such as optical) properties of the sensing material.

3. Micro and nanostructuring of sensing layers for SAW gas sensors

Considerable efforts have been made to study the influence of the structures and morphologies of the sensing layer materials on SAW gas sensors' performance. Amongst the sensitive materials employed for SAW gas sensing, nanostructured materials have drawn increased attention in the last few years. Recently, nanostructured sensing layers with various morphologies, including porous structures, hollow structures, and one-dimensional nanoscale structures, have been considered as exceptional approaches for optimizing the sensing performance and sparked intensive research interests.

It is generally accepted that the morphology of the sensitive layer, especially the porosity, plays a critical role in the performance of the SAW gas sensor. The porous structure ensures a large-area contact between gas molecules and the sensing material, which provides excellent responses of the sensors.[70] The gas detection capability of the SAW sensor is also affected by the uniformity and compactness of the film. For example, Han *et al.*[71] and Chen *et al.*[72] prepared hierarchical WO_3 flower-like spheres and single-crystal WO_3 nanosheets to detect triethanolamine. The former study showed excellent performance and a low theoretical limit of detection of 83 ppb for triethanolamine, which was better than the latter one. The reason for the former's apparent outstanding sensing performance was that this unique nanostructure facilitated the activities of surface reactions and accelerated the diffusion of triethanolamine molecules into the sensing layers. Particularly, hierarchical structures with large surface-to-volume ratios and porous features provide abundant active sites, and the loosely connected WO_3 nanosheets facilitate the gas transportation and thus promote the response and recovery speeds.

Compared to one or two-dimensional nanomaterials, three-dimensional structures possess much larger effectively specific surface areas and porosities, which are beneficial to the diffusion of gas molecules and transport of electrons/holes.[73] For example, Wang *et al.*[74] synthesized four different WO_3 structures (nanorods, spheres, sea urchins and flowers respectively) as sensing materials to detect VOCs. Among these, the three-dimensional sea urchin morphology exhibited the best sensitivity in a low concentration. This can be explained by the fact that the large area exposure of the crystal surfaces affected the pre-adsorption of negative oxygen ions and also provided more channels for the faster gas diffusion, thus enhancing the gas sensing performance. Morphologies of different types of sensing materials can be easily optimized using various types of synthesis methods, reaction conditions and solution concentrations. For example, Xu *et al.*[75] adjusted the concentration of the raw materials to change the shape of WO_3. With a suitable concentration of $NaHSO_4$, three-dimensional flower-like WO_3 was produced and possessed large specific areas and hierarchically porous structures, which provided more channels for fast gas diffusion and increased active sites for adsorbing target gases easily. This unique structure showed the highest sensing response compared with the other types of morphologies and the response value was at ~96 at the ethanol concentration of 35 ppm. In addition, Wang *et al.*[76] found that Sb-doping changed the morphology of SnO_2 from nanowires to nanosheets. The structural features of nanosheets increased the number of surface active sites and defects, thereby greatly improving the responses and sensitivity of gas sensors. It should also be pointed out that the introduction of foreign ions in SnO_2 leads to changes in the growth state of SnO_2. In particular, if Sb^{5+} replaces Sn^{4+}, the electrons provided by Sb^{5+} are easily captured by NO_2, causing the SnO_2 to enter a depleted state which improves gas responses. If Sb^{3+} is replaced with

Sn^{4+}, a certain concentration of O vacancy is induced by Sb-doping, which can be ionized into second-order ionized oxygen vacancy $V_{\ddot{O}}$. More free electrons can be produced which ban be captured by NO_2 to further enhance the performance of the gas sensor. Therefore, doping has become a good methodology to improve the gas sensing performance of SAW sensors.

For constructing well-organized micro- and nanoscale morphologies, strategies using various advanced synthetic methods have been applied for preparing high-performance SAW gas sensor materials. For example, pulse laser deposition is often used in the preparation of sensor materials because of its multiple tunable parameters such as atmospheric pressure, laser power, substrate temperature, and flexible geometry. Recently, Miu *et al.*[77] used pulsed laser deposition to synthesize ZnO films with different porosities by controlling various parameters such as the gas pressure inside the deposition chamber, the number of pulses and pulse duration and the substrate temperature. The ZnO films deposited using the optimal parameters show a larger density of pores and a better sensing response. This is because the higher deposition pressure leads to an increase in plasma density and increased collisions among the ablated species, thus resulting in the formation of relatively smaller nanoparticles in the target–substrate region. Liu *et al.*[78] designed and successfully prepared aperture-controllable three-dimensional mesoporous ZnO nanostructures to detect acetone and methanol. These unique structures with large macropores demonstrated much better gas sensing performance than ZnO nanoparticles, because the very large cavity pores provide numerous spaces for gas diffusion and a synergistic effect of electron transportation and electron density of gas molecules.[79] Specifically, mesoporous ZnO structures provide excellent transportation channels and surface accessibility for gas molecules to diffuse into the inner part of nanostructures whereas the absence of these macropores in those nanoparticles significantly slows down the gas responses due to the existence of long and tortuous pathways for gas permeation and diffusion. Shu *et al.*[80] explored the relationships and mechanisms between the frequency shift of the SAW gas sensor and the surface morphology of ZnO thin film. They found that grain size was dependent on the grain diffusion rate and the deposition rate of ZnO crystals, which were determined by the deposition temperature. Their experimental results demonstrated that the deposited porous ZnO films show a large frequency response (310 kHz) to a concentration of 40% O_2 and good stability for a long period at a high temperature under the deposition conditions (850 °C). Therefore, selecting suitable methods and process parameters is necessary for synthesizing porous materials to further improve the sensing performance of the SAW device. Other synthetic methods such as electrospinning, magnetron sputtering and hydrothermal growth have also been applied for the deposition of dense or porous structures and controlling the distributions of incorporated crystals or nanoparticles. In the next section, we will focus on several types of nanostructured sensing materials such as semiconductor metal oxides, carbon-based and polymer-based materials, and discuss in detail the influences of their structural morphologies and different modifications on their sensing performance.

4. Sensing materials for SAW gas sensors

In SAW sensing technology, development and integration of new sensing materials have been a focused research area. These nanostructured SAW sensors can be used for a large range of applications, such as the detection of VOCs, poisonous gases, or explosive gases. The commonly used sensing materials have been listed in the following categories.

4.1 Semiconductor metal oxides

An important category of sensing layer materials for SAW sensors is semiconductor metal oxides, which are applied in many fields such as luminescent materials and gas sensing materials. Many nanostructured semiconductor metal oxides have a large surface area due to their ultrafine crystals or particles, which can adsorb more target analytes on their surfaces, providing stronger signals and causing more measurable responses. Besides, the abundant free electrons on their surface, after being triggered by external sources, can effectively interact with reducing or oxidative gas molecules, which is beneficial to improving the sensing efficiency.[3,14,17,26,81–84] For SAW based gas sensors, the following metal oxides have been extensively applied.

4.1.1 ZnO-based sensing layer. ZnO is an important representative of such sensitive materials in the field of gas sensors. Its relatively simple synthesis process can control the morphology and generation of oxygen vacancies, which are advantageous in the field of sensors for gas molecule adsorption.[35,85,86] Meanwhile, ZnO is an n-type II–IV element, and a wide and direct band gap semiconductor with a bandgap of about 3.37 eV and a large excitation binding energy (60 meV).[35,87–89] Its high electron mobility makes it the most favored material in the field of optoelectronics and sensors.

Raj *et al.*[90] prepared a series of different metal oxides (ZnO, TeO_2, SnO_2 and TiO_2) with the same thickness (40 nm) by using the RF sputtering technique for the detection of NH_3. The deposited ZnO thin film had the highest sensitivity to NH_3 compared with other oxides. This can be attributed to the numerous native defects related to the zinc interstitials, zinc vacancies, oxygen interstitials, oxygen vacancies and antisite defects that exist in the ZnO thin film, which are beneficial for the better performance than the other oxide films.[91,92] The authors sequentially studied the influences of the thickness of the ZnO sensing layer (20–40 nm) on the SAW sensing characteristics, and found that with the increase in film thickness, both the crystallite size and the average roughness of films are decreased. Their results also showed that the number of adsorption sites for the targeted gas molecules increases with increase in the thickness of the sensing layer from 20 to 40 nm, and the best sensing performance was obtained with the thickness of 40 nm. Rana *et al.*[93] successfully fabricated a ZnO thin film based sensing layer on a quartz SAW device to detect

NO_2 gas, and selectively detected trace NO_2 concentration (400 ppb to 16 ppm) due to the deposited ZnO thin films with small particle sizes, which led to larger specific surface areas and was favorable for efficient adsorption and desorption of target gas molecules on their surfaces.

The sensitivity of the sensor is strongly related to the ZnO deposited volume on the specific surface area, and also dependent on its morphology. Marcu *et al.*[94] synthesized ZnO nanowires and ZnO thin films onto quartz substrates using a laser beam process and measured the SAW device's responses to various concentrations of hydrogen and deuterium gases. They designed and synthesized ZnO nanowires (300 nm and 600 nm-long) and thin films (100 nm and 200 nm-thick). High frequency responses and rapid responses for nanowires at a low concentration were found. In particular, the nanowire (600 nm) showed a higher sensitivity (0.015 Hz ppm^{-1}) and lower limit of detection (2117 ppm) for the detection of hydrogen.[94] Meanwhile, the response time (9–15 s, the time to reach 90% of the maximal signal) of the nanowire sensors was longer than that of thin film-based SAW sensors (2–3 s). The recovery time (*i.e.*, the time required for the response signal to return to 90% of the original baseline signal when the target gas is removed) for the nanowire sensors (6–9 s) was shorter than that for the film sensor (7–11 s). Meanwhile, Marcu *et al.*[95] also applied ZnO nanowires (888 nm long) prepared *via* a vapor–liquid–solid technique as the sensing layers which exhibited a higher sensitivity (0.062 Hz ppm^{-1}) for hydrogen detection than ZnO thin films (0.01 Hz ppm^{-1}).

ZnO nanorods have also been proved to exhibit a better sensing performance than the thin film when they are deposited onto the SAW devices. As reported by Li *et al.*,[96] ZnO nanorods with large specific surface areas were synthesized by a seed layer-free hydrothermal method and showed excellent sensitivity, repeatability and stability in the detection of NH_3. Fig. 3a and b show schematic illustrations of the measurement system and the morphology of ZnO nanorods, respectively. Fig. 3c shows that the frequency shifts of two morphological materials were observed under different concentrations of ammonia gas. Notably, the one with nanorods showed a larger frequency shift at the same gas concentrations because ZnO nanorods possess large specific surface areas that can adsorb more oxygen species and react with more ammonia molecules than the ZnO film. The sensors based on ZnO nanorods also manifested stable responses in a certain range of NH_3 concentrations for 60 days (Fig. 3d).

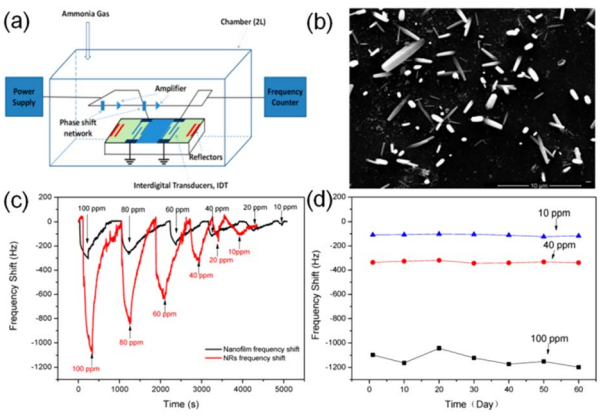

Fig. 3 (a) Schematic diagram of ammonia gas. (b) Top-view morphology image of ZnO nanorods. (c) Frequency shifts of SAW devices based on ZnO nanorods to varying concentrations of ammonia. (d) Frequency shifts of SAW devices based on ZnO nanorods to various concentrations of NH_3 gas for 60 days. Reproduced with permission from ref. 96, ©MDPI journals 2017.

Metal doped ZnO has also been applied as the sensing layer in SAW devices. Platinum (Pt), as a noble metal, has attracted extensive attention in the chemical and physical fields such as catalysis and sensing. Huang *et al.*[97] used Pt doped ZnO nanorods as the selective sensing layer for the SAW device in H_2 detection. The frequency shift for detecting a H_2 concentration variation of 6000 ppm was 26 kHz, which was superior to pure ZnO nanorods and ZnO thin films. Particularly, it took less than 15 s to reach about 90% of the steady state, and the recovery time was about 2–3 min. This remarkable sensing performance is mainly due to the doping of Pt, which acts as a catalyst to speed up the reaction rate.

Palladium (Pd) has excellent hydrogen adsorption properties, the highest hydrogen solubility at atmospheric pressure as well as thermodynamically favored H_2 dissociation.[98,99] Viespe *et al.*[100] designed a Pd/ZnO bilayer structure for H_2 detection based on a quartz SAW sensor operated at room temperature. The sensor structure combined the hydrogen absorption and diffusion properties of Pd with the excellent diffusion properties of the nanoporous Pd film, which resulted in increased amounts of hydrogen gas molecules reaching the Pd/ZnO interface. At this interface, the ZnO surface conductivity is highly sensitive to the adsorbed species, thus improving the detection sensitivity for hydrogen. Therefore, this sensor showed a higher sensitivity (0.51 Hz ppm^{-1}) and a better limit of detection (59 ppm) than the single ZnO films and single Pd films.

As it is well known, oxygen vacancies, generated by elemental doping or chemical reduction, have a critical role in the gas sensing performance of semiconductor metal oxide materials due to the increased free carrier concentration.[101,102] For example, Ghosh *et al.*[103] discovered that the performance of a ZnO thin film coated langasite SAW sensor could be improved by calcium (Ca) doping of ZnO in CO_2 detection. There are two mechanisms of frequency responses for these Ca doped ZnO sensing. The first one is the mass loading effect produced by the reaction of CO_2 gas with O^- species to form CO_3^{2-}. The second one is the increase in conductivity owing to the catalytic effect of Ca, and the influence of the increase in conductivity is predominant. It is noteworthy that the SAW sensor is also sensitive to H_2 and CO gas. Shu *et al.*[104] reported that the doping of Fe element could obviously change the morphology of the ZnO sensitive film and improve the gas sensing performance in O_2 detection. With the increase of Fe content in the film, both the size and amount of the nanosheets are increased. The proportion of Fe^{3+} ions is increased, which results in an increased content of Fe_{Zn}. This will result in the substitution of Zn^{2+} ions by Fe^{3+} ions, thus generating more free electrons.

Composites of ZnO and other materials have recently been explored for examining the dependence of the response of a composite SAW sensor to oxidizing or reducing gases. The improvement in sensing performance using these composites has been ascribed to many factors. These include: (1) electronic effects such as the separation of charge carriers[105] and the manipulation of the depletion layer;[106] (2) chemical effects such as reduced activation energy[107] and synergistic surface reactions;[108] and (3) physical geometric effects such as grain shrinkage[109] and surface area expansion.[110] For example, Tang *et al.*[111] synthesized a ZnO–Al_2O_3 nanocomposite coated on the quartz SAW device using a sol–gel method for H_2S detection. The composite with a porous structure had a good affinity to H_2S, and thus could selectively adsorb H_2S, which led to an increase in the elastic modulus of the bi-layer, and a positive frequency shift (15 kHz ppm^{-1}). The elastic loading was mainly due to the fact that the newly formed ZnS had a higher molar mass and a lower density compared with original ZnO nanoparticles. The key sensing mechanism is that as the ZnO–Al_2O_3 layer has a mesoporous structure and a rough surface, a large amount of H_2S molecules can enter deeply inside the layer diffusing through the porous structures and then react with ZnO nanoparticles. Tang *et al.*[112] also reported that a ZnO/SiO_2 bi-layer nanofilm synthesized by a sol–gel process was much more sensitive than the single layer films due to their appropriate sheet conductivity. With the increase of the top thickness of the ZnO layer in the bi-layer film structure, the sensitivity of the SAW sensor was significantly improved. Particularly, bi-layer nanofilms of ZnO had a better frequency response (a frequency shift of 2 kHz at the NH_3 concentration of 30 ppm), while the response time and recovery time were much higher than other thin films. The sensing mechanism can be explained as follows. Oxygen molecules are adsorbed on the surface of the top ZnO layer owing to the van der Waals force, and the adsorbed oxygen molecules capture the free electrons on the surface to form a depletion layer. When the film is exposed to NH_3 gas, some NH_3 molecules diffuse and even penetrate into the film because of the film's porous structure. These molecules react with oxygen species causing numerous electrons to be released back into the depletion layer. These electrons will recombine with some of the holes, thus changing the conductivity of the ZnO layer. Consequently, this results in a negative shift in frequency. Wang *et al.*[113] also reported ZnO/SiO_2 composite films with different molar ratios, which were synthesized using a sol–gel method. Experiments showed that when the ratio of ZnO to SiO_2 in the composite films is 1 : 2, the SAW sensor showed the best sensing performance. At an injected NH_3 concentration of 10 ppm, the response of the SAW sensor was 1.132 kHz, which was much higher than that of the sensor based on a pure ZnO film. The excellent performance of this device is attributed to the enhanced adsorption of NH_3 molecules and unique surface reactions due to the existence of silica on the surface of the composite film.

There are also studies using a composite layer by combining ZnO with InO_x for the SAW gas sensor. The oxygen vacancies in the InO_x film serve as donors and the sample's conductivity is changed by controlling the concentration of oxygen deficiencies.[114] InO_x layers deposited on XZ cut $LiNbO_3$ with a 1.2 μm ZnO guiding layer were also reported,[115] and a large frequency shift of positive 91 kHz for 2 ppm of NO_2 and negative 319 kHz for 1% H_2 in synthetic air were observed for the 40 nm InO_x layer. Nieuwenhuizen *et al.*[116] used a quartz SAW sensor coated with ZnO–SiO_2–Si layers and a dual delay-line oscillator system to detect the NO_2 gas. Results clearly showed that the sensing performance of an NO_2 SAW sensor of this type using copper phthalocyanine (CuPC) as the chemical interface was excellent.

4.1.2 SnO_2-based sensing layer. SnO_2 is one of the most stable oxides among n-type oxides widely used for semiconductor gas sensors. It has a higher mobility of electrons and higher stability compared with ZnO, and thus SnO_2 has been explored as a good semiconductor for gas sensors.[117,118] In 2015, Luo *et al.*[119] applied SnO_2 films synthesized by an aqueous sol–gel technique as an efficient H_2S sensing layer in a quartz SAW device. They examined the gas sensing properties of the SAW sensors under different concentrations of H_2S and different temperatures using a testing system as shown in Fig. 4a. Their experimental results showed that SnO_2 thin layer had a maximum frequency response of 112.232 kHz (Fig. 4b) at the H_2S concentration of 68.5 ppm and the low of detection limitation was 1.7 ppm. Fig. 4c shows the responses of gas sensors with different SnO_2 film thicknesses to 68.5 ppm of H_2S at 120 °C. It clearly shows that the sensor with a film thickness of 275 nm exhibited the highest sensitivity (1.6384 kHz ppm^{-1}). Moreover, the authors also found that the electric effect was dominant in the sensing mechanism of this SAW sensor. Fig. 4d shows three-dimensional relationships between the relative frequency shift and the sheet conductivity of the SnO_2 films with different thicknesses before and after contacting the H_2S gas. When the sheet conductivities of the film with a thickness of 275 nm (operated at 120 °C) were increased, the frequency shift caused became significantly increased. They also used SnO_2 as the sensitive film of the SAW gas sensor to detect H_2S.[120]

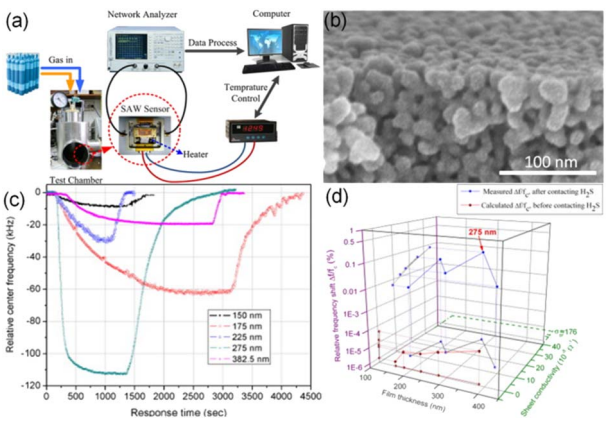

Fig. 4 (a) Manufacturing process of the SAW gas sensors. (b) Morphology images of the SnO_2 films on quartz. (c) Sensor response to 68.5 ppm of H_2S for samples with different film thicknesses at 120 °C. Three-dimensional plots of the relationships among the relative frequency shift, the sheet conductivity of the films and (d) film thickness. Reproduced with permission from ref. 119, ©Elsevier 2015.

Raj *et al.*[121] used SnO_2 thin film as the sensing layer, which was coated on a quartz SAW oscillator to detect NO_2 gas. They reported that the film thickness is the most important factor affecting the sensor performance. This is because with the increase of its thickness, the average roughness of the SnO_2 thin films increased and the average porosity of the sensing film also increased, which causes adsorption of more targeted molecules on the SnO_2 thin films. Therefore, with increase in the film thickness, the frequency of the SAW sensor was increased leading to enhanced sensing responses with a fast response time (~2 s) and recovery time (~45 s).

Nevertheless, SAW sensors using the pure SnO_2 sensing layer often suffer from poor selectivity, and the operation temperature is also quite high.[122] Therefore, researchers have been exploring various methods to enhance its performance, such as doping with other elements, modifying the microstructures, and using composite structures. As described earlier, noble metals can be efficiently used to improve the performance of gas sensors. For instance, Yang *et al.*[123] prepared a SnO_2 thin film using a sol–gel method with doped Pd nanoparticles. Pd catalytic nanoparticles increased the quantity of O_2 species and the adsorption capacity of H_2 gas on the surface of SnO_2, resulting in a decrease of initial electrical conductivity and an increase of electrical conductivity in H_2 gas. This bi-layer structure enhanced the H_2 gas sensing properties of composite thin films with a frequency shift of 115.9 kHz at the H_2 concentration of 2000 ppm. Furthermore, this SAW sensor displayed fast response (1 s) and recovery time (512 s).

Constantinoiu *et al.*[124] deposited p-type Co_3O_4 on n-type SnO_2 thin films to improve the SAW gas sensing performance of a single SnO_2 thin film layer for the detection of NH_3. Two different types of oxides form a heterojunction, which is the active area for the adsorption of oxygen species, thus improving the sensitivity of the sensor.[105] Apparently, compared with a single layer of Co_3O_4 or SnO_2 thin film layer, the sensitivity (3.33 Hz ppm^{-1}), limit of detection (9 ppm), response (100–120 s) and recovery time (30–50 s) of the sensor in the case of NH_3 detection were improved. Meanwhile, p-type CuO was also deposited on an n-type SnO_2 thin film layer to enhance the performance of H_2S detection.[125] The p–n junctions were modified by the CuS formation, which was formed by CuO particles and H_2S, and the conductivity of the films was increased drastically and then the operating frequency was decreased. Thus, high sensitivity (16.9 kHz ppm^{-1}), excellent selectivity, fast response time (55 s) and recovery time (45 s), and superior repeatability were obtained. The above examples show that the combination of other metal oxides or single noble metal layers with SnO_2 can effectively improve the SAW gas sensing performance.

4.1.3 WO_3-based sensing layer. WO_3 is another important and promising candidate to be used as a sensing element in gas analysis. Moreover, WO_3 film also shows electrochromic properties and is suitable for H_2 sensing in a photodetector device.[126–128] Wen *et al.*[129] developed a NO_2 gas sensor which consisted of a dual track SAW device and a microporous network WO_3 film. They reported that there were numerous microporous networks in the WO_3 film since polyvinylpyrrolidone was used in the preparation, and these porous structures effectively adsorbed NO_2 molecules at room temperature by means of the mass loading effects. When the SAW sensor was exposed to the NO_2 concentration of 3 ppm, the frequency response was up to 0.185 kHz with good reproducibility and stability. According to the previous theories, the sensor response was significantly increased with a decrease in the thickness of the WO_3 lamellae and was well-correlated with its thickness. Kida *et al.*[130] fabricated lamellar-structured WO_3 particles by acidification of Na_2WO_4 and subsequent calcination of the resulting precipitates. The obtained material was spin-coated on the quartz SAW device as a sensing layer to detect NO_2, and the device exhibited a good SAW sensing performance. The excellent performance was attributed to the use of smaller lamellae which decreased the electrical resistance of the device and allowed the detection of NO_2 in a wide concentration range.

As discussed above, noble metals, such as Pd, Ag, Au, and Pt, are the most common catalyst activators used in semiconductor metal oxide gas sensors, which can significantly strengthen the reactions between the target gas and oxide surface and reduce the response/recovery times. Ippolito *et al.*[131] reported that a WO_3 selective layer modified with Pt or Au exhibited a much higher sensitivity compared to a layered SAW sensor that employed only a bare WO_3 selective layer. Particularly, they obtained large frequency shifts of 705 and 118 kHz towards 1% H_2 in air for the Au-WO_3 and Pt-WO_3 SAW sensors, respectively, and the bare WO_3 selective layer only showed a shift of 25.8 kHz. Jakubik *et al.*[132] also compared the SAW sensing performance of WO_3 and bilayer Pd-WO_3 in the detection of H_2. Their experimental results showed that adding a Pd thin layer onto the WO_3 layer greatly improved the sensor's sensitivity to H_2 with a concentration from 0.5% to 4% in dry air. In addition, Miu *et al.*[133] deposited Pd modified WO_3 film onto an ST-X cut quartz SAW sensor to detect H_2. Their experiments identified that the combination of nanoporous Pd (which was efficient in dissociating H_2) and WO_3 thin films of nanostructures endowed the SAW device with a good sensing performance.

4.1.4 TiO_2-based sensing layer. Among the known semiconducting metal oxides, nanostructured TiO_2 is one of the most investigated materials for gas sensors, pigments in coating, electrocatalysis, energy storage, photovoltaic and photocatalysis applications because of its low-cost, high band gap energy, excellent chemical stability, and environmental friendliness.[134–138] Rella *et al.*[139] synthesized TiO_2 nanoparticle thin film using a novel chemical route and deposited it on Si and Al_2O_3 substrates by matrix assisted pulsed laser evaporation to detect acetone and ethanol solid-state gas using the quartz SAW device. A uniform distribution of TiO_2 nanoparticle layer with an average particle size of about 10 nm was obtained and this thin sensing layer has round-shaped clusters, with a high degree of roughness and porosity. It is well-known that the single semiconductor metal oxide cannot achieve high sensitivity and selectivity due to the low chemical reactivity. Therefore, functionalization of semiconductor metal oxides to improve both the precise selectivity and high sensitivity of semiconductor metal oxide-based gas sensors has been widely

explored. For example, Tang *et al.*[140] prepared pure SiO_2, TiO_2 and a SiO_2–TiO_2 bi-layer composite (Fig. 5a) using a sol–gel method and coated them on a quartz SAW resonator using a spin coating technique. The sensing performance and mechanisms of the SAW NH_3 sensor were systematically investigated. They concluded that the bi-layer composite formed by these two oxides had a highly porous structure with more compact pores and micro-cracks, and meanwhile the particle size was larger than that of pure SiO_2 and TiO_2. The compact pores and micro-cracks served as the channels for target gas molecules to diffuse fast into the membrane structure; consequently, porous states formed on the surface acted as the absorption sites for target gases, which was conducive to enhancing the sensing performance. Fig. 5b shows the responses or frequency shifts of the pure SiO_2, TiO_2 and bi-layer composite SiO_2–TiO_2 sensors, respectively; the composite sensing layer showed a larger frequency response, which can be ascribed to the fact that the composite more easily adsorbed NH_3 in the air. The sensing mechanisms on the sensing film surface for interacting with NH_3 are schematically illustrated in Fig. 5c. The first mechanism is that this film is able to capture the water molecules in the surrounding environment. The second one is that the absorbed water can serve as the active sites for trapping NH_3, as NH_3 can easily dissolve in water, thus increasing the mass of the bi-layer composite. The third one suggests that the hydroxyl groups are formed by the catalytic condensation reaction of the adsorbed NH_3 on the surface of the bi-layer film. The composite SiO_2–TiO_2 films had a much better sensitivity to NH_3 at a low concentration level (1 ppm) with a response of 2 kHz (Fig. 5d and e), and also showed fast response and recovery times (Fig. 5f), excellent selectivity, stability and reproducibility.

Constantinoiu *et al.*[141] deposited a Pd/TiO_2 composite thin film onto the quartz SAW device to detect the concentration of H_2. They obtained sensitive films with different morphologies by changing the O_2 and Ar pressures in the pulsed laser deposition chamber. With increase of Pd pressure, the composite films possessed a more porous structure, and more H_2 molecules were adsorbed and dissociated which resulted in the improved performance of the Pd/TiO_2 composite thin films compared to the pure TiO_2 thin films. Therefore, Pd/TiO_2 thin films with a porous morphology had a larger frequency response (1.8 kHz at 2% H_2 concentration), higher sensitivity (0.10 Hz ppm^{-1}) and a lower limit of detection (1210 ppm) than pure TiO_2 thin films. The experiment further confirmed that efficiency modification can greatly improve the sensing performance of single semiconductor metal oxides.

4.1.5 Other types of sensing layers. Apart from the above discussed semiconductor metal oxides, other sensing layer materials also exhibit excellent sensing performance. For example, Li *et al.*[142] explored nanoparticulate CuO films as a sensing layer of a SAW sensor for the detection of H_2S (Fig. 6a). The key mechanism is that CuO thin films (Fig. 6b) are able to capture H_2S molecules in the surrounding environment and then react with these molecules to generate Cu_2S or CuS particles on their surface. Compared with original CuO particles, the new phases formed by chemical reactions had modified physical and chemical properties, such as increased mass and elastic modulus, and decreased electrical conductivity. The performance of the CuO-based SAW sensor was tested with the H_2S concentration range from 0.5 to 10 ppm at room temperature and 75% relative humidity. The obtained results are displayed in Fig. 6c. The information from Fig. 6d shows that the response time and recovery time are positively correlated with H_2S

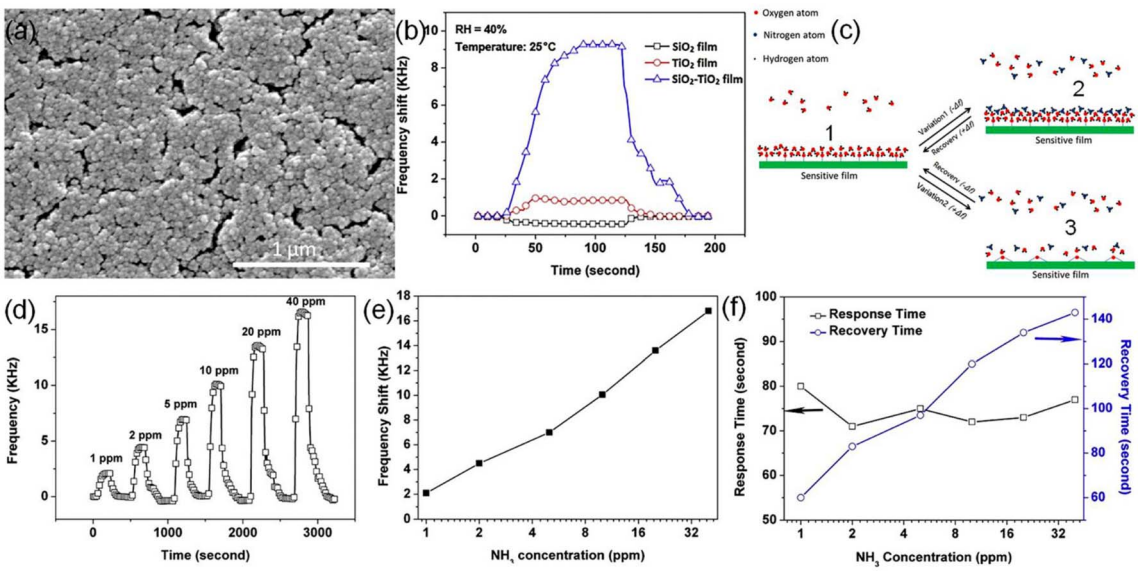

Fig. 5 (a) The surface morphology images of SiO_2–TiO_2 films. (b) Frequency responses of the SAW sensor based on SiO_2, TiO_2 and SiO_2–TiO_2 films to 10 ppm NH_3. (c) Sensing principle of a film with hydroxyl groups. (1) The sensing film in ambient air, H_2O is adsorbed on the film. (2) Variation 1: NH_3 is absorbed in the H_2O on the film. (3) The film is condensation after adsorbing NH_3. (d) Dynamic frequency responses to NH_3 of various concentrations for the sensor based on SiO_2–TiO_2 film. (e) Frequency response as a function of NH_3 concentration. (f) Response and recovery times as a function of NH_3 concentration. Reproduced with permission from ref. 140, ©Elsevier 2018.

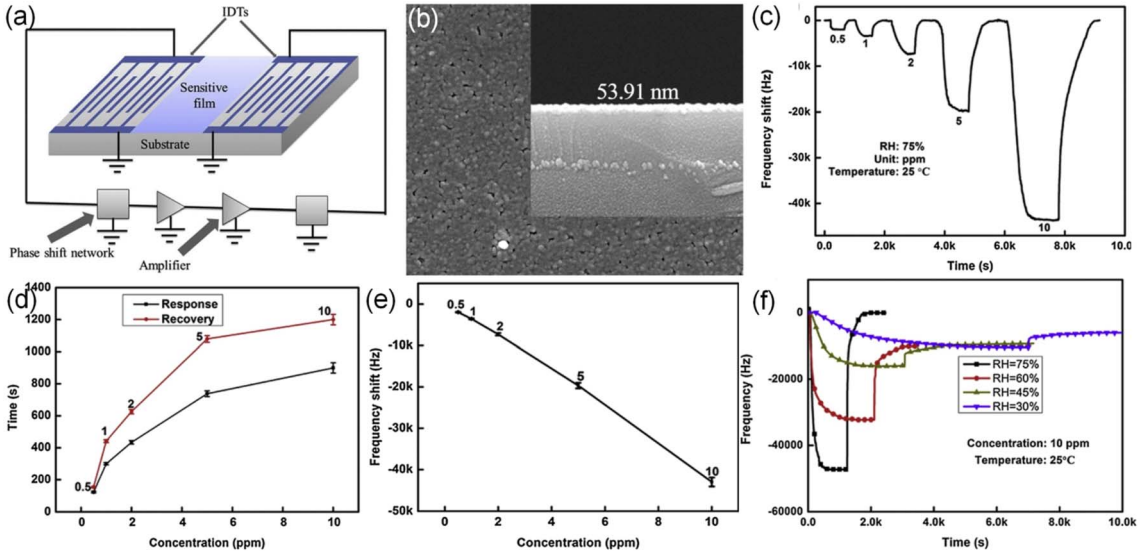

Fig. 6 (a) Schematic diagram of a SAW sensor. (b) Morphology image of the top-view and cross-section view of as-synthesized CuO film. (c) Dynamic response of the sensor to H_2S of various concentrations with RH = 75% at 25 °C. (d) The response and recovery time *versus* the concentration. (e) The response (frequency shift) to the concentration, together with error bars. (f) Dynamic response of the sensor to 10 ppm H_2S with various RH at 25 °C. Reproduced with permission from ref. 142, ©Elsevier 2019.

concentration. The relationships between concentration and frequency shifts are shown in Fig. 6e. The data were highly fitted with a linear curve, confirming that relative humidity affects the response of the SAW sensor (Fig. 6f). Moreover, excellent sensing performance of the CuO film sensing layer was achieved; for instance, the frequency shift was −1.2 kHz when the H_2S concentration was 500 ppb.

Tang *et al.*[143] synthesized a CuO–Al_2O_3 composite film through optimizing the single CuO thin film for the detection of H_2S gas. CuO nanoparticles served as the active sites and adsorbed more H_2S molecules. Meanwhile, Al_2O_3 nanoparticles could easily form the uniform and mesoporous structure. Their synergistic effect enhanced the sensing performance of the SAW sensors. Compared with pure CuO nanoparticles, the composite film showed a lower detection limit (0.005 ppm) and higher sensitivity (-16.3 kHz ppm^{-1}) to H_2S gas at the concentration of 5 ppb to 100 ppm. Kiriakidis *et al.*[144] prepared a crystalline InO_x layer using DC magnetron sputtering to detect the sensitivity of the SAW sensor to ozone gases, and studied the sensing properties of different thicknesses of oxides to NO_2, reducing gases such as H_2, and ozone. The 20 nm InO_x coated on the quartz SAW device showed a 73.562 kHz frequency shift for 510 ppb of NO_2 at an operating temperature of 168 °C, and the frequency responses towards H_2 gas concentrations of 600–10000 ppm were in the range of 78.5–319.4 kHz. H_2, as a reducing gas, increased the conductivity of InO_x, thus the acoustic wave velocity was decreased, and this was the main reason for the observed decrease in the oscillation frequency in the presence of H_2. At an operation temperature of 123 °C, frequency shifts of 42.7 kHz for 50 ppb and 52.7 kHz for 100 ppb of ozone were detected.

Dewan *et al.*[145] reported that TeO_{2+y} ($y = 0$–1) thin films were sensitive to the NO_x gas. They studied the influence of the sensing layer thickness on the response characteristics, and a thicker TeO_2 film was found to result in enhanced sensitivity of the SAW device. Tang *et al.*[146] found that a Co_3O_4/SiO_2 composite layer could act as a sensing film when applied in SAW sensors for the detection of NH_3. Material characterization studies, such as scanning electron microscopy (SEM) and atomic force microscopy (AFM), indicated that the films showed porous structures, which was beneficial to the selective adsorption and reaction with gas molecules. In addition, the existence of SiO_2 was also demonstrated to enhance the NH_3 sensing property of the composite sensor significantly due to the porous structure of pristine SiO_2 film. The loading of 50% Co_3O_4 produced the roughest surface morphology and displayed a positive frequency shift of 3.5 kHz to NH_3 at a concentration of 1 ppm and showed excellent selectivity, stability and reproducibility at room temperature. Wang *et al.*[147] also reported a porous Fe_2O_3–SiO_2 layer coated on the surface of a quartz SAW device to detect H_2S. A porous structure facilitates the diffusion of gases into the sensing layer, thereby enabling the full interactions between the layer and gas molecules. In this experiment, Fe_2O_3 nanoparticles effectively adsorbed and reacted with H_2S molecules because the porous SiO_2 served as a support to disperse nanoparticles, thus it manifested a fast response shift of −4.4 kHz at the H_2S concentration of 100 ppm.

In summary, different semiconductor metal oxide-based sensing materials have different reactivities to the targeted gases. Structures and morphologies are the key points that affect the sensing performance of SAW sensors. Large surface areas of semiconductor metal oxides can provide numerous reaction contact areas between the gas sensing materials and target gases. Porous nanostructures, assembled from numerous small grains with nanoscale voids and pores, are useful to enhance the sensitivity. Besides, modifying semiconductor

metal oxides by doping is also an effective way to improve the performance of SAW sensors.

4.2 Carbon-based sensing materials

Carbon-based nanomaterials, including carbon nanotubes and graphene oxides, exhibit excellent performance in sensing application owing to their high surface area, mechanical properties and outstanding electrical conductivity.[148,149] In this section, we will discuss two micro/nanostructure examples of carbon-based sensing materials as sensing layers applied to SAW sensors, including carbon nanotubes and graphene oxides.

4.2.1 Carbon nanotube-based sensing layer. Carbon nanotubes have outstanding mechanical, physicochemical, thermal and electrical properties. Moreover, carbon nanotubes possess huge surface areas, which make them prospective candidates for sensing applications.[150,151] For example, Sivaramakrishnan *et al.*[152] applied carbon nanotube films coated on a quartz SAW device (Fig. 7a) to monitor the CO_2 gas concentration by detecting the change in acoustoelectric coupling between the piezoelectric SAW substrate and the carbon nanotube film deposited on the acoustic pathway. Their studies showed an alternative technology of SAW-based carbon nanotube sensors for carbon dioxide sensing in respiratory monitoring.

Single-walled carbon nanotubes (SWCNTs) are potential gas sensing materials with prominent properties such as hollow structures, high specific surface areas, one-dimensional tubular nanostructures, high electron mobility and high chemical reactivity.[153,154] It was reported that multi-wall carbon nanotubes (MWNTs) made the sensing film more porous, increasing the contact areas between the gas molecules and sensing material, thus enhancing the performance of traditional gas-sensitive materials at room temperature.[155,156] Penza *et al.*[157] fabricated quartz SAW sensors coated by either SWCNTs or MWCNTs for chemical detection of volatile organic compounds, such as ethanol, ethylacetate and toluene. They reported that the sensitivity of the SWCNT-based sensor in the detection of ethanol (6.89 kHz ppm^{-1}) was higher than those of ethylacetate (3.32 kHz ppm^{-1}) and toluene (3.17 kHz ppm^{-1}). There are two reasons for this phenomenon.[157] The first is that the SWCNTs exhibited a larger surface area for gas detection than MWCNTs. The second is the key role of oxygen. When it comes into contact with carbon nanotubes under ambient conditions, oxygen is chemisorbed and serves as a chemical mediator between carbon nanotubes and the organic solvents used. Penza *et al.*[158] also designed and synthesized a SWCNT-based sensing layers and coated it onto a 36° Y-cut X-propagation $LiTaO_3$ piezoelectric SAW substrate to detect various gases. In their study, the SWCNT-based nanocomposite acted as the sensing layer and was deposited on SAW oscillators (Fig. 7b and c). The sensing of NO_2, NH_3 and H_2 gases was monitored by the changes of the SAW device's phase velocities, because the mass-loading, elastic-loading and electric-loading caused by gas adsorption can lead to a change in the SAW phase velocity. Fig. 7d–f show that when exposed to a certain concentration of gas, the layered SAW sensor adsorbed the gas molecules, and the phase velocity

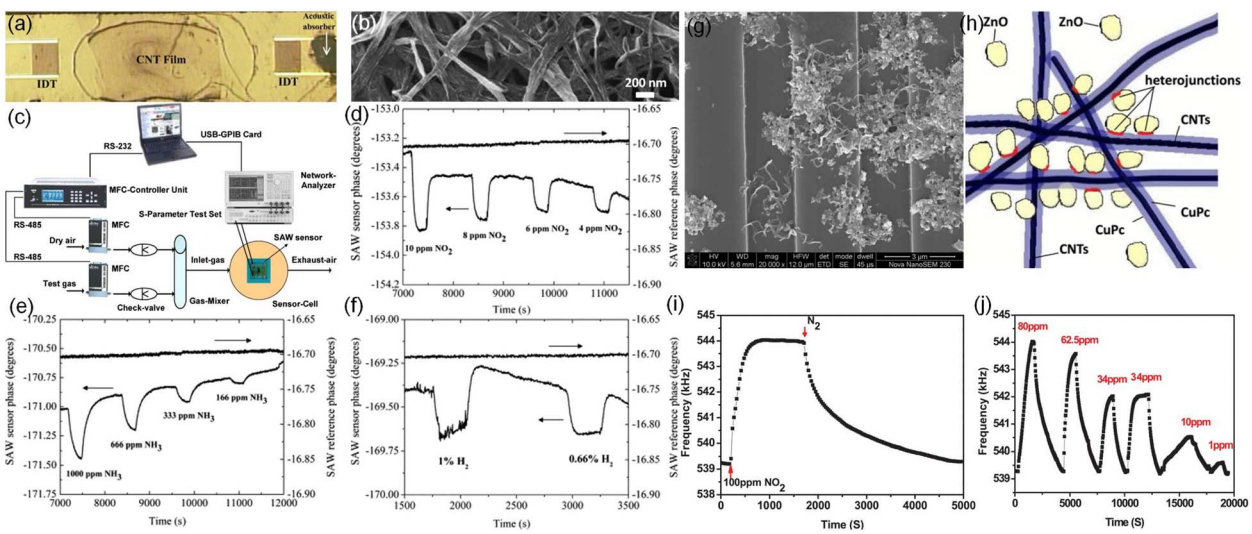

Fig. 7 (a) CNT-coated SAW delay line; reproduced with permission from ref. 152, ©Elsevier 2008. (b) High magnification of Langmuir–Blodgett (LB) 75 wt% nanocomposite film of SWCNTs-in-cadmium arachidate (CdA). (c) Scheme of the experimental setup used for gas sensing testing of SAW devices. (d) SAW phase response of the uncoated reference $ZnO/LiTaO_3$ device and the $ZnO/LiTaO_3$ Love-mode sensor coated with 10 monolayers of 75 wt% SWCNT-in-CdA LB nanocomposite film towards NO_2 gas at room temperature. (e) SAW phase response of the uncoated reference $ZnO/LiTaO_3$ device and the $ZnO/LiTaO_3$ Love-mode sensor coated with 10 monolayers of 75 wt% SWCNT-in-CdA LB nanocomposite film towards NH_3 gas, at room temperature. (f) SAW phase response of the uncoated reference $ZnO/LiTaO_3$ device and the $ZnO/LiTaO_3$ Love-mode sensor coated with 10 monolayers of 75 wt% SWCNT-in-CdA LB nanocomposite film towards H_2 gas, at room temperature. Reproduced with permission from ref. 158, ©Elsevier 2007. (g) SEM image of the CuPc/ZnO film based on the MWNT framework. (h) Hetero-structure of ZnO and CuPc/MWNTs. (i) ZnO doped CuPc/MWNT film SAW sensor's response to 100 ppm NO_2. (j) ZnO doped CuPc/MWNT film SAW sensor's response to 1–80 ppm NO_2. Reproduced with permission from ref. 167, ©IEEE Xplore 2015.

of the SAW sensor was decreased until the saturation occurred in the sensitive layer. Therefore, the sensor signal was restored to its initial base line when the test gas was exposed to dry air.

Recent studies showed that the SAW sensors' sensing performance of carbon nanotubes can be improved by using polymer coatings,[159] carbon nanotube-based nano-composites,[160] certain functional groups,[161] and physical and chemical modifications using metal nanoclusters.[162,163] For example, Asad *et al.*[164] applied SWCNTs as a sensing layer decorated with Cu nanoparticles (denoted as Cu NP-SWCNTs) to detect H_2S gas. Cu nanoparticles have been reported to act as modified layer materials which greatly enhanced the sensing performance of ZnO[165] and WO_3.[166] Cu NP-SWCNTs were reported to show good sensing results as the coated SAW device showed a larger frequency shift to H_2S (~260 kHz at the gas concentration of 10 ppm) compared with others at the optimum operating temperature (175 °C). Additionally, at this temperature and the H_2S concentration of 300 ppm, the response time and recovery time of the sensor were 7 and 9 s, respectively. Duan *et al.*[167] also reported that MWCNTs decorated with phthalocyanine copper (CuPc) and ZnO showed good performance, which could be attributed to the unique heterojunction structures (Fig. 7g and h), which increased the carriers' lifetime. The electron depletion of the p–n heterojunction increased the ability of surface active sites to adsorb NO_2 molecules. The authors also tested the performance of the SAW sensor at 100 ppm concentration of NO_2 and the response times at different concentrations of NO_2. The results obtained are shown in Fig. 7i and j, respectively, and the composites displayed high sensitivity (0.0505 kHz ppm^{-1}), good linearity and fast response time. Furthermore, carbon nanotubes functionalized using polymers are promising candidates to obtain new sensitive layers for gas detection in order to improve the sensitivity and selectivity of the gas sensors.[168,169]

4.2.2 GO-based sensing layer. Graphene oxide (GO) is an important nanomaterial for SAW sensor applications because it combines 2D structural features of graphene with the presence of oxygen-containing functional groups (hydroxyl, epoxide and carbonyl groups) that interact with a great variety of analytes.[170–172] Sayago *et al.*[173] presented a Love-wave SAW sensor deposited with the GO layers to detect different concentrations for simulants of chemical warfare agents below the median lethal doses. When tested using various chemical warfare agents, the quartz SAW device with GO layers show a higher sensitivity (3.087 kHz ppm^{-1}) to dimethyl-methylphosphonate than to the others (the sensitivities of 1,2-dichloroethane, dipropylene glycol monomethyl ether, and dimethylacetamide were 0.0009, 0.0069, and 0.76 kHz ppm^{-1}, respectively), with a limit of detection as low as 9 ppb. It was because the multiple oxygen-containing functionalities, such as epoxy, hydroxyl and carbonyl groups on the surface of GO sheets, can be connected with PO groups to form stronger hydrogen bonds. Tang *et al.*[174] reported GO spin-coating on an ST-cut quartz Love mode SAW substrate to detect NH_3. Multifunctional groups such as hydroxyl and epoxy ones on the surface of GO film can adsorb more NH_3 molecules. The NH_3 molecules could be easily adsorbed and filled within the gaps between different GO atomic layers, thus increasing the stiffness of the film, and finally leading to a positive frequency shift of 620 Hz at a lower NH_3 concentration of 500 ppb.

As mentioned above, the catalytic properties of Pd and its sensitivity towards H_2 in the case of the SAW devices can be improved by doping with Pd. Li *et al.*[175] proposed a H_2 SAW sensor based on the decoration of GO by Pd nanoparticles on an AlN/Si layered structure. This H_2 SAW sensor showed higher sensitivity (~9.5 times) and lower cross-sensitivity towards NO_2 compared to those based on pure GO. Hydrogen molecules are dissociated into atoms on the Pd surface and the resulting hydrogen atoms are dissolved in the Pd/GO composite with a high solubility, and the composite film provided larger exposure areas and penetration depths for hydrogen molecules, which contributed to a good sensing performance. Arsat *et al.*[176] reported the deposition of thin graphene-like nanosheets on a quartz SAW interdigitated transducer to assess the sensing performance. However, GO that was incompletely reduced by hydrazine was covered with hydroxyl, carbonyl epoxide and other functional groups on its surface. These functional groups not only passivated the GO surface, but also reduced the affinity of the surface with adsorbate molecules.[176] Therefore, an ideal GO-based SAW sensor may have better sensing characteristics than the one involving incompletely reduced GO.

As discussed above, carbon-based materials due to their excellent thermal, electronic and optical properties as well as high electron mobilities have become key sensing nanomaterials for SAW gas sensor applications. It is worth noting that the hybrids of carbon materials and nanoparticles of noble metals and oxides are one of the main research directions of SAW gas sensors, owing to their superior sensing performance.

4.3 Polymers-based sensing materials

Polymers are frequently used as active layers in SAW sensor devices due to their large range of capabilities.[177–179] Nowadays, polymers are readily available and easily tunable in terms of their functional groups in polymeric backbones; as a result, they are often used to detect different analyte vapors.[180,181]

Amati *et al.*[182] summarized various organic polymers which have been applied to SAW sensors with good sensitivities, selectivities and response times for several concentrations of toluene, acetone and dichloromethane. Rabus *et al.*[183] described a SAW passive wireless sensor coated with a polymer thin film to monitor the presence of H_2S in the subsurface environment. The combination of SAW and ground penetrating radar was reported and thus the presence of gas in the underground could be detected with the sensor, even at a depth of 1 meter. However, it has a disadvantage that the wireless detection signal to noise ratio is degraded by radiofrequency signal attenuation when propagating through the soil leading to poorer detection limits than in the wired configuration. In the following sections, we will discuss several typical polymer-based active sensing materials applied to SAW gas sensors.

4.3.1 PANI-based sensing layer. Polyaniline (PANI) exhibits a good sensing performance because of its large specific surface areas and interconnected network structures. Shen *et al.*[184]

investigated a SAW sensor coated with a PANI film to monitor the presence of NH_3. The concentration of NH_3 was 20.45 ppm, the frequency shift was 1.79 kHz, and the response time was less than 150 s. The performance could be attributed to the fact that NH_3 molecules are easily adsorbed by H_2O molecules, and more NH_3 molecules are capable of diffusing into their films and reacting with the active site of PANI chains. Specifically, the sensing film becomes deprotonated, and the deprotonation rate depends on the concentration of NH_3, which in turn results in a change of the resistance.

The sensing performance of polymer-based SAW gas sensors can be improved by enhancing the electrical and physical properties of polymers by using various dopants and the modification of their structures.[185] Nanofibers have a cylindrical morphology and will form porous structures when deposited as thin films. The synthesis of modified PANI nanofibers was found to have a remarkable influence on the SAW device sensitivity.[186] Hence, hydrochloric acid (HCl) and camphor sulfonic acid (CSA) as dopant acids were used in the synthesis processes to obtain PANI nanofibers with an average diameter of 30 and 50 nm (Fig. 8a and b, respectively) to detect the sensitivity of the SAW sensor to H_2.[187] Fig. 8c shows that the responses were 3 kHz and 14.6 kHz toward 1% of H_2 for HCl and CSA doped PANI nanofiber sensors, respectively. The dynamic responses of the CSA- and HCl-doped PANI nanofiber sensors to different H_2 concentrations are shown in Fig. 8d and e. The HCl doped sensor showed faster response and recovery times compared to the CSA doped sensor for all concentrations of H_2 (Fig. 8f). Three possible reasons for these phenomena were reported. (1) The diameter of the nanofibers provided a different amount of surface area for H_2 interaction. (2) The differences in volatility and mobility of the dopants might give rise to variable speeds of reaction. (3) There might be variation in the doping level of the dried films.[187]

Sadek *et al.*[188] reported a PANI/In_2O_3 nanofiber composite based SAW gas sensor to detect H_2. The activation of the hydrogen by In_2O_3 makes the composite to absorb more H_2, which enhanced the sensing performance. Besides, facilitated by In_2O_3, the hydrogen dissociates and interacts with the PANI backbone, leading to either a doping type response or chain alignment, which also contributes to a good sensing performance.

4.3.2 TEA-based sensing layer. Liu *et al.*[189] reported a quartz SAW device deposited with triethanolamine (TEA) to detect H_2S at room temperature, owing to the high efficiency adsorption of TEA and the existence of van der Waals' interactions and hydrogen bonds with H_2S molecules. The sensing mechanism was proposed as follows: the adsorption of TEA towards H_2S modulated the propagation of SAW, and the corresponding phase changes were converted into voltage signals proportional to the concentration of H_2S which were collected as the sensor signals. The obtained experimental results showed that fast response time (7 s), high sensitivity (0.152 mV ppm^{-1}) and a lower detection limit (0.15 ppm) were achieved with the H_2S concentration of 4 ppm at room temperature. However, an undesirable coating loss caused by thermal evaporation of TEA at a high temperature and high flow rate was observed, thus affecting the sensing performance. Qin *et al.*[190] reported a SAW gas sensor coated with TEA modified with boric acid to detect SO_2. The SAW device with the modified TEA shows better performance than that using pure TEA, which was attributed to the reaction of boric acid and TEA-derived nitrogen atoms in the cage structure that possessed a lone pair of electrons, making it more sensitive to SO_2.

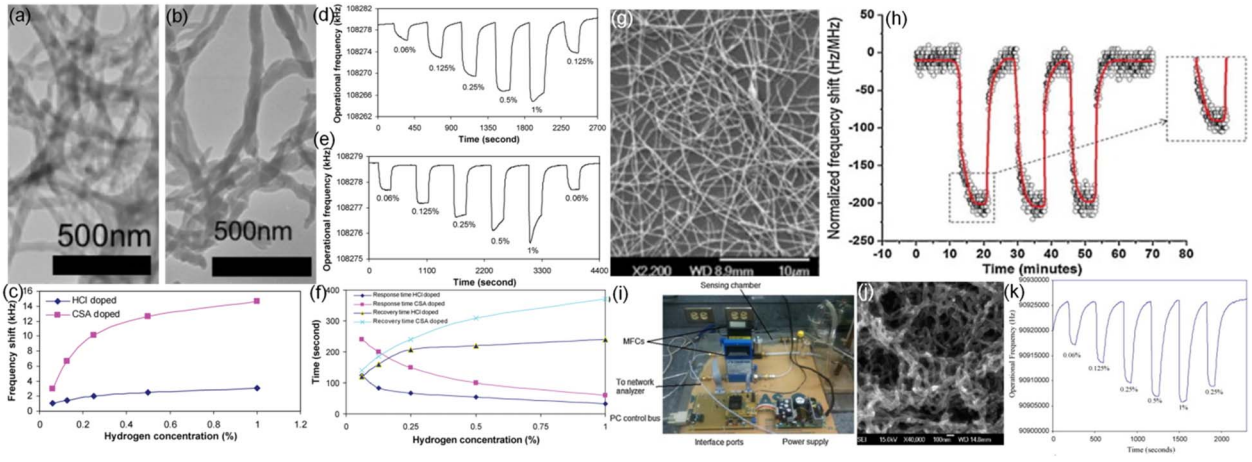

Fig. 8 TEM images: (a) HCl-doped and (b) CSA-doped polyaniline nanofibers. (c) Frequency shift (in kilohertz) *versus* H_2 gas concentrations (in percent) at room temperature. (d) Dynamic response of a CSA-doped and (e) HCl-doped polyaniline nanofiber based ZnO/64° YX $LiNbO_3$ SAW sensor toward H_2 at room temperature. (f) Response and recovery times (in seconds) *versus* H_2 gas concentrations (in percent) at room temperature. Reproduced with permission from ref. 187, ©IEEE Xplore 2007. (g) SEM picture of the top view of electrospun PEO nanofibers on the SAW device substrate. (h) Nanofibrous film SAW sensor response to hydrogen peroxide vapor (30%) (solid lines are the average fitting lines). (i) Actual experimental setup of the SAW sensor measurement system; reproduced with permission from ref. 191, ©Elsevier 2011. (j) SEM image of polypyrrole nanofibers. (k) The dynamic response of the sensor towards different concentrations of H_2. Reproduced with permission from ref. 193, ©Elsevier 2008.

4.3.3 PEO-based sensing layer. Methylene chains in polyethylene oxide (PEO) possess an antioxidant nature and increase the lifetime of the films, which not only enhances the mechanical properties of the polymeric film but also increases the elasticity of the suspension liquid during the spraying process. It is a good choice for the SAW gas sensor no matter if it is in the selection of materials or in the preparation of the spin coating solution. For example, Liu *et al.*[191] reported a SAW sensing layer which was synthesized using ultrafine (100–300 nm) PEO fibers (Fig. 8g). The nanofibrous film achieved a high surface area to volume ratio, which could not only offer more adsorption sites for vapor molecules, but also shorten the diffusion length of vapor molecules into polymer materials, and these merits are favorable to enhancing the performance of the sensor. The electrospun nanofiber SAW sensor showed excellent repeatability with variations lower than 5%. The frequency shifts of the SAW sensor are shown in Fig. 8h, and the test environment is shown in Fig. 8i.

4.3.4 PPy-based sensing layer. Polypyrrole (PPy) is an attractive conducting polymer in SAW sensor design due to its easy polymerization into films, its relative stability and high electrical conductivity.[192] Mashat *et al.*[193] previously presented a quartz SAW device deposited with PPy nanofibers for the detection of H_2 and NO_2 at room temperature. PPy nanofibers were prepared by a template-free chemical route and characterized by SEM, Fourier transform infrared spectroscopy (FT-IR) and transmission electron microscopy (TEM) techniques, respectively. The information from Fig. 8j indicates that the length of the nanofibers was several microns and the average diameter was 18 nm. SAW gas sensing tests using the device with a PPy layer showed that when exposed to a gas concentration of 1% H_2 and 2.1 ppm NO_2, the frequency deviation was 20.194 kHz and 4.5 kHz, respectively, and meanwhile the SAW sensor had a good repeatability (Fig. 8k).

Chen *et al.*[194] developed SAW NH_3 gas sensors based on different layers of PPy and Pt doped PPy layers. The doping of Pt was achieved by immersing substrates with the PPy film. Compared with different layers of PPy, it was found that the device with two layers of PPy film showed the best performance among the devices with different layers of PPy films. The rough surface enabled the film to adsorb more NH_3 molecules, and meanwhile, the Pt catalyst enhanced the reaction between the NH_3 and PPy, causing larger decrease of PPy's resistance and thus leading to a larger electrical loading effect. Furthermore, the response and stability of the device with two layers of PPy could be further improved by doping Pt. Chen *et al.*[194] showed that it could be possible to use other noble metals, such as Au, Ag, and Pt for doping PPy films as the sensing materials for the SAW sensor.

Pasupuleti *et al.*[195] reported that the quartz SAW device with a sensing layer of PPy modified poly(3,4-ethylenedioxythiophene) polystyrene sulfonate (PEDOT:PSS) hybrid nanocomposite exhibited a high sensitivity of ~9.38 kHz with a positive frequency shift and a low detection limit (~231 ppb) towards CO (100 ppm) gas. The outstanding performance is attributed to the sensing layer's high porosity, large surface area, and abundant OH and amine functionalizing groups. Moreover, the synergetic effect of the p–p hybrid heterojunction, which can act as active surface sites, further improved the effective absorption of CO gas molecules. The addition of PPy enhanced the conductivity of the composite and there was a strong interfacial charge interaction at the hybrid heterojunction interface, which is further beneficial to improve the gas reaction kinetics.[195]

4.3.5 PVP-based sensing layer. Polyvinylpyrrolidone (PVP) has many extraordinary physical and chemical properties, such as high thermal and chemical stability, non-toxicity and excellent solubility in water and many organic solvents, which make it a suitable material for gas detection.[196] Besides, PVP, a nonconducting polymer, has also been reported to be sensitive to ammonia and aliphatic amines, since its carbonyl groups and nitrogen sites are considered as hydrogen bond acceptors.[197] Recently, He *et al.*[198] prepared PVP fibers by electrospinning and investigated the effects of the concentration of PVP solution and electrode-to-collector distance on the morphology of the electrospun PVP fibers. Electrospinning processes of such a PVP layer can be varied by changing the electric field intensity and solution viscosity, thereby affecting its morphology and the SAW sensing performance.[199] When the concentration of PVP solution was 58%, smooth and uniform nanofibers were obtained, which possessed a larger surface-to-volume ratio than that obtained using the other concentration of PVP. In the gas sensing test, the frequency shift was about 5.6 kHz at the H_2 concentration of 1% and it showed a fast response time (120 s) and recovery time (200 s). This outstanding sensing performance can be attributed to the unique chemical and physical structures of the PVP. Particularly, PVP can act as a hydrogen bond acceptor due to the existence of both carbonyl groups (CO) and nitrogen (N:) sites.[200] H_2 acted as the hydrogen bond donor and can be easily adsorbed by PVP fibers causing a significant mass loading. Chee *et al.*[201] investigated the gas sensing performance of a PVP/MWNT composite based SAW sensor. The effect of the amount of PVP on the morphologies of the composite was investigated because PVP is well known to prevent agglomeration of the particles and stabilize the particle sizes. Characterization results showed that the morphology obtained with a large amount of PVP is nanofibers, while that obtained with a small amount of PVP is nanoparticles dispersed in MWNTs. Meanwhile, experimental results also revealed that the sensing performance of the composite could be mainly attributed to the hydrogen bond connection between PVP and H_2. Therefore, PVP has a great potential for the detection of H_2. Matatagui *et al.*[199] also used PVP fibers prepared using an electrospinning technique as a sensitive layer of the SAW sensors to detect VOCs. The process voltages were changed to obtain a series of different diameters of PVP. With a higher voltage applied, the diameter of nanofibers was lower and possessed a larger active surface which can adsorb more toluene molecules. The sensing sensitivity of PVP (3.25 Hz ppm^{-1}) to toluene was also reported to be superior to that reported for PEO (0.45 Hz ppm^{-1}).[202]

To sum up, the unique tunable electrical properties, along with easy synthesis, structural diversity, facial functionalization

as well as flexibility of these polymer sensing materials are suitable for gas sensing. Attention should be paid to their low sensitivity and poor stability, which hinder their practical sensing applications. As listed above, various strategies have been proposed to enhance the sensing performance, including increasing the active surface area, redox doping and surface functionalization. Therefore, it is crucial to continuously develop high-performance polymer materials for the application of SAW gas sensors.

4.4 Other types of common sensing materials

Apart from the sensing materials reported above, many other types of sensing layer materials also exhibit excellent sensing performance with respect to SAW sensors.

4.4.1 Cellulose-based sensing layer. Cellulose has various exceptional characteristics such as large specific area (~250 $m^2 g^{-1}$) and abundant surface hydroxyl groups, which are beneficial for gas sensing. In recent years, researchers have successively developed cellulose as a sensing layer coated on a quartz SAW device to detect the sensitivity to various gases. For instance, Tang *et al.*[203] reported that cellulose nano-crystals (CNCs) could be used as a sensitive and selective layer in SAW sensors for HCl gas detection. The CNCs have been found to possess abundant hydroxyl groups on their surfaces, which acted as the perfect adsorption sites for H_2O and also greatly promoted the adsorption of HCl gas. The sensor showed an ability to detect HCl at a low concentration of 1 ppm with a response of −2 kHz, and the response could reach as high as −80 kHz when the concentration of HCl gas was increased to 200 ppm.[203] Wang *et al.*[204] synthesized a bi-layer composite film composed of bacterial cellulose and polyethyleneimine (PEI), which were deposited on a quartz SAW device to detect formaldehyde. The bacterial cellulose films possessed ultrafine fibrous and filamentous network structures, and the unique structure provided a large amount of adsorption sites for the PEI particles. Meanwhile, the hydrogen bonds formed between the hydroxyl group on the surface of bacterial cellulose and the amine group of PEI were found to prevent the aggregation of PEI particles, ensure the uniform distribution of PEI on the bacterial cellulose films, and enhance the adsorption effect of formaldehyde gas. Therefore, the SAW sensor exhibited good sensing performance with a frequency response of 35.6 kHz with a formaldehyde concentration of 10 ppm.

4.4.2 Hydroxylate-based sensing layer. Tang *et al.*[205] synthesized hydroxyl-rich AlO_xOH_y films on a quartz SAW device using a sol–gel method with different spin coating cycles and temperatures (Fig. 9a–f). The fabricated SAW sensors showed negative frequency shifts when exposed to HCl gas. The reason was attributed to the increased weight of sensitive films induced by the adsorption of HCl assisted by the hydroxyl groups and H_2O captured on the films. The sensing mechanism of the SAW HCl sensor based on AlO_xOH_y films is illustrated in Fig. 9g. The sensor with a 198 nm-thick AlO_xOH_y film annealed at 300 °C showed a response of ~−1.4 kHz to HCl at a low concentration level (0.05 ppm) in an environment with a temperature of 25 °C (Fig. 9h and i). The response and recovery times as a function of

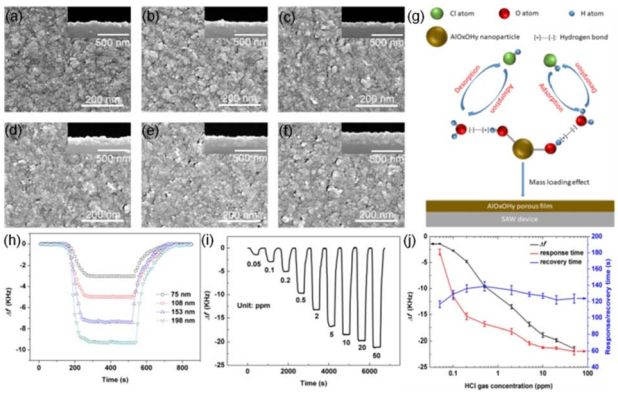

Fig. 9 (a) SEM images of (a) F-1-150, (b) F-1-300, (c) F-1-450, (d) F-2-300, (e) F-3-300, and (f) F-4-300. Different spin coating cycles and temperatures. Inset images are the cross-sectional views of films. (g) The proposed sensing mechanism of the SAW HCl sensor based on AlO_xOH_y films. (h) The dynamic responses of sensors based on F-1-300, F-2-300, F-3-300 and F-4-300 coated resonators to 0.5 ppm HCl. (i) The dynamic responses of the sensor based on F-4-300 to HCl of various concentrations. (j) The response, response time and recovery time as a function of the concentration of HCl (log scale). Reproduced with permission from ref. 205, ©Elsevier 2020.

HCl gas concentration are shown in Fig. 9j. As can be seen, the recovery time was changed inconspicuously whereas the response time significantly increased when the concentration of HCl increased from 0.05 to 50 ppm.

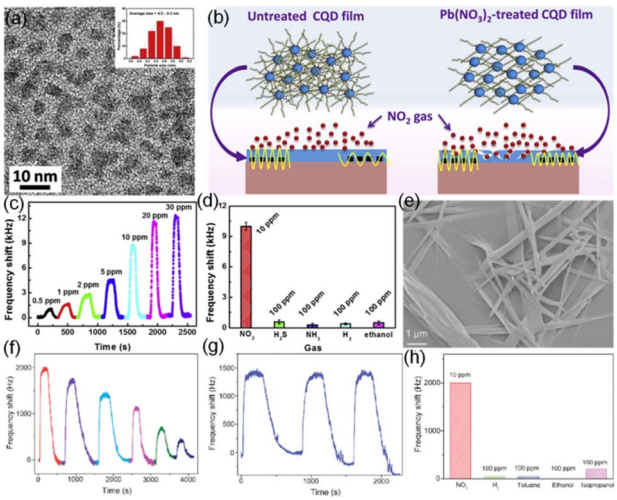

Fig. 10 (a) TEM of the synthesized PbS CQDs. Inset is the size distribution of the sample. (b) Schematic diagrams of the gas sensing mechanism of the SAW gas sensors based on the untreated and $Pb(NO_3)_2$-treated PbS CQD films. (c) Transient response curves of the $Pb(NO_3)_2$-treated PbS CQD-based SAW sensor to 0.5–30 ppm NO_2 gas at room temperature. (d) The selectivity of the sensor; reproduced with permission from ref. 212, ©Elsevier 2019. (e) SEM of Bi_2S_3 nanobelts. (f) The dynamic sensing responses of the sensor to 1.2–10 ppm NO_2 gas. (g) Response curves of the Bi_2S_3 nanobelts based SAW sensor to 6 ppm NO_2 at room temperature. (h) The selectivity of the sensor towards diverse gases. Reproduced with permission from ref. 217, ©IEEE Xplore 2021.

Table 1 Summary of sensing materials of SAW gas sensors

Material	Target gas	C (ppm)	Response (kHz)	T_{res}/T_{rec} (s)	LOD (ppm)	Ref.
ZnO films	NH_3	120 000	376.9	—	—	90
ZnO films	NH_3	—	—	21/180	—	91
ZnO films	NH_3	7500	4.2	15/—	—	92
ZnO film	NO_2	0.4	6	—	0.4	93
ZnO nanowires	H_2	1	0.000015	9/6	2117	94
ZnO nanowires	H_2	100	0.0062	—	2253	95
ZnO nanorods	NH_3	100	−1.094	151/568	—	96
Pt–ZnO nanorods	H_2	6000	26	15/120	—	97
Pd/ZnO films	H_2	1	0.00051	12–16/—	59	100
Ca–ZnO films	CO_2	25 000	2.469	87/132	—	103
Zn_xFe_yO films	O_2	—	258	201/∼320	—	104
ZnO/Al_2O_3 films	H_2S	0.01	∼0.5	—	—	111
ZnO/SiO_2 films	NH_3	30	2	38/30	—	112
ZnO/SiO_2 films	NH_3	10	1.132	∼70/∼60	—	113
InO_x–$ZnO/LiNbO_3$	NO_2	2.125	91	180/360	—	115
CuPc–ZnO–SiO_2–Si	NO_2	1	0.92	420/—	—	116
SnO_2 films	H_2S	68.5	112.232	—	1.7125	119
SnO_2 films	H_2S	13.7	—	142/602	1.5802	120
SnO_2 films	NO_2	20	∼30	2/45	—	121
Pd–SnO_2 films	H_2	2000	115.9	<1/583	—	123
SnO_2/Co_3O_4 films	NH_3	—	—	100/30	9	124
SnO_2/CuO films	H_2S	20	230	55/45	∼0.53	125
WO_3 films	NO_2	3	0.185	—	3	129
WO_3 particles	NO_2	—	—	—	—	130
Pt–WO_3 films	H_2	10 000	118	240/480	—	131
Au–WO_3 films	H_2	10 000	705	180/360	—	131
Pd/WO_3 films	H_2	40 000	2.4	∼100/100	—	132
TiO_2 particles	Acetone	—	—	240/—	—	139
SiO_2–TiO_2 films	NH_3	1	2	—/60	1	140
Pd/TiO_2 films	H_2	20 000	1.8	—	1210	141
CuO films	H_2S	0.5	−1.2	—	0.5	142
CuO–Al_2O_3 film	H_2S	1	−16.3	—	0.005	143
InO_x films	NO_2	8.5	91	—	—	144
TeO_{2+y} films	NO_x	0.27 vol%	263	—	—	145
Co_3O_4/SiO_2 films	NH_3	1	3.5	—	—	146
Fe_2O_3–SiO_2 films	H_2S	100	−4.4	<200/—	—	147
CNTs	CO_2	—	—	—	—	152
SWCNTs	Ethanol	1	6.89	120/—	1.3	157
SWCNTs	NH_3	—	—	—	30	158
Cu NP-SWCNTs	H_2S	10	∼260	7/9	—	164
CuPc/MWNTs	NO_2	100	5	∼300/1800	—	167
PANI/CNTs	H_2	100	0.32	420/420	10 000	168
Polymer/CNTs	Toluene, octane	100, 100	0.101, 0.438	40/60	9.2/1.7	169
GO	DMMP, DPGME	1, 1	3.087, 0.76	900/780, 480/490	0.009, 0.04	173
GO	NH_3	5	6.2	250/700	0.5	174
Pd/GO	H_2	1000	2.07	7/7	—	175
Graphene-like nano-sheets	H_2, CO	10000, 1000	5.8, 8.5	12/<60, 300/1200	—	176
Polymers	Toluene	100	0.0502	—	4	182
Polymers	H_2S	200 000	—	—	—	183
PANI film	NH_3	1.79	20.45	<150/—	25	184
PANI	NH_3	1.79	20.45	<150/—	25	187
PANI/In_2O_3	H_2	10 000	11	30/40	—	188
TEA	H_2S	—	—	—	0.15	189
TEA	SO_2	1	0.08	60/240	—	190
PEO fibers	Isopropanol	100 000	−0.767	60/60	—	191
PPy nanofibers	H_2, NO_2	10000, 2.1	20, 4.5	39/219, (133/298)	—	193
Pt/PPy	NH_3	100	0.175	—	—	194
PPy@PEDOT:PSS	CO	100	∼9.38	121/138	∼0.231	195
PVP fibers	H_2	10 000	5.6	120/200	—	198
PVP fiber	Toluene	10	30	—	10	199
Cellulose nano-crystals	HCl	1/5	−2/−10	∼45/∼500	—	203
Cellulose/polyethyleneimine	Formaldehyde	10	35.6	34/28	0.1	204
AlO_xOH_y films	HCl	0.05	∼−0.0014	—/60	0.05	205

Table 1 (*Contd.*)

Material	Target gas	C (ppm)	Response (kHz)	T_{res}/T_{rec} (s)	LOD (ppm)	Ref.
Pd nanoparticles	H_2	1600	—	—	—	206
Pd films	H_2	—	—	—	50	207
ZnS films	NH_3	20	~3.8	45/148	—	211
PbS CQDs	NO_2	10	9.8	45/58	0.032	212
SnS CQDs	NO_2	10	~−1.8	180/446	0.052	213
Bi_2S_3 nanobelts	NO_2	10	2	—	0.017	217

4.4.3 Noble metal-based sensing layer. Noble metals are well known for their unique large surface area-to-volume ratio, optical and electronic properties, and high stability. Hence, they are widely used in various applications such as catalytic systems, fuel cells and sensors. Take the noble metal Pd as an example, many studies reported that the dissociation of H_2 on Pd is thermodynamically favorable because the combination of H_2 and Pd easily leads to the formation of PdH_x. The formation of Pd–H occurs mainly through the following processes, *e.g.*, physisorption, chemisorption and dissociation of H_2 on the surface, introduction of hydrogen atoms on the Pd surface and diffusion of H atoms into the bulk, and finally the palladium hydride formation.[98,99] Meanwhile, the absorption of H_2 can cause strain formation in the lattices of Pd, and further change the electrical properties.[121] Consequently, Pd can be applied as the sensing material for H_2 gas detection. For example, Sil *et al.*[206] reported the use of Pd nanoparticles (5–20 nm) as the sensing layer coated on quartz SAW devices to detect H_2. Experiments confirmed that exposure to H_2 induces lattice expansion in Pd, which brought the nanoparticles together more tightly and enhanced the sensing performance. Moreover, the decreased binding energy of Pd lowered the miscibility gaps, and a set of surface adsorption sites for hydrogen adsorption appeared, which enhanced the hydrogen sensing property. Amico *et al.*[207] deposited Pd thin films on a quartz SAW device to detect the concentration of H_2. The interparticle distance in the Pd nanoparticle films provided spaces for hydrogen to induce morphological changes. Pd nanoparticles also exhibited a higher specific surface area thus providing more adsorption active sites, enabling the hydrogen to diffuse in and out more readily, increasing the rate at which the sensor could respond to a change in hydrogen vapor concentration and reducing hysteresis. All of the aforementioned properties made Pd nanoparticles exhibit better performance than Pd films.

Au thin film as a sensing layer coated on the SAW device also exhibited excellent sensing performance, for example, to detect chloroform.[208] Laser-deposited Au immobilization layers with different porosities were obtained which further improved the sensing performance. The results show that the porous Au layer showed a much larger frequency shift (26 kHz) under the same conditions compared with those of other morphologies. This excellent performance can be ascribed to the high surface to volume ratio, which is beneficial to the gas diffusion.

4.4.4 Sulfide-based sensing layer. Compared with metal oxides, metal sulfides have a wider forbidden band and better thermal stability,[209,210] suitable for SAW sensors. For example, the crystal structure of ZnS, with a wide band gap of 3.72 eV, is similar to that of ZnO and has abundant sulfur vacancies on its surface. Long *et al.*[211] developed mucosal-like ZnS nanostructures which were applied as a sensing layer for a SAW NH_3 sensor. When the ZnS film was exposed to a NH_3 atmosphere, the active O^{2-} ions that reacted with the NH_3 molecules were adsorbed on the surface of the film to release electrons, which led to a decreased depletion layer and increased conductivity of the film. The good sensing performance is mainly attributed to its large specific surface areas and increased active sites on its surface, which make ZnS films adsorb more NH_3 molecules. Li *et al.*[212] deposited $Pb(NO_3)_2$-treated PbS colloidal quantum dots (CQDs, Fig. 10a) onto a quartz SAW device to detect the sensing performance of NO_2. Compared with PbS CQDs, the $Pb(NO_3)_2$-treated PbS CQDs SAW sensor displayed faster response and recovery times (45 s and 58 s, respectively), as well as a larger positive frequency shift (9.8 kHz). It can be ascribed to the excellent performance of $Pb(NO_3)_2$-treated PbS CQDs with a porous structure, which could trap more NO_2 molecules (Fig. 10b). Meanwhile, the sensing response of $Pb(NO_3)_2$-treated PbS CQD-based SAW sensor to 0.5–30 ppm NO_2 gas at room temperature was tested (Fig. 10c) and it showed good stability and selectivity (Fig. 10d). Effective combination of PbS and CQDs is the key reason for the improved performance because these CQDs have large specific surface areas that contribute to a large amount of active sites for adsorbing target gases. However, Pb has cost, environmental and health problems which limit its widespread use. Thus, it is necessary to explore SAW gas sensors based on sensing materials with low toxicity but still showing a high performance. Li *et al.*[213] reported SnS CQDs as the sensing layer deposited onto a quartz SAW sensor to detect NO_2. The SnS CQDs, with their ultrafine particles (5 nm), large surface areas and numerous adsorbed active sites, were capable of detecting a low concentration of NO_2 gas (10 ppm) and showed good selectivity and repeatability.

Narrow band gap semiconductors such as Bi_2S_3 (1.3–1.7 eV) have been widely studied due to their application in optoelectronic devices, hydrogen storage materials, solar cells, and gas sensors.[214–216] Luo *et al.*[217] deposited one-dimensional Bi_2S_3 nanobelts onto the sensing area of an ST-cut quartz SAW device for NO_2 gas detection at room temperature. Fig. 10e shows that these Bi_2S_3 nanobelts with porous structures are beneficial to adsorb NO_2 gas molecules, thereby improving the sensing performance. The Bi_2S_3 nanobelts SAW sensor exhibited

a positive frequency shift of 2 kHz toward 10 ppm NO_2 with good sensitivity, stability and selectivity (Fig. 10f–h).

5. Conclusions and future perspectives

Design and application of novel sensing materials provides a valuable method for the development of SAW gas sensors. This review summarizes the advances of sensing materials towards gas sensing applications based on SAW technology in recent years. The basic sensing mechanism of SAW gas sensors and the evolution of sensing parameters have been discussed. A wide range of materials (including semiconductor metal oxides, carbon-based materials, and polymers) as efficient sensing layers used in the SAW based gas sensors are reviewed in Table 1. The synthesis strategy, composition and structure–activity relationship of these sensing materials are also discussed.

Although considerable advances have been made in recent years towards the synthesis of sensing materials and improvements of SAW gas sensors, there are still many challenges to be tackled and various issues to be explored. Some of these future directions are listed below.

(i) One of the main challenges with the use of SAW gas sensors is the ability to maintain long-term stability under varying environmental conditions, such as temperature and humidity. For the last few years, a great deal of studies have explored the effects of humidity and temperature on the sensitivity of SAW gas sensors.[218,219] It should be pointed out that the sensing performance of SAW sensors in the literature is based on the results obtained under controlled laboratory conditions. However, in practical applications, the gas sensing performance of the SAW sensors would be changed significantly with the variations of the external environment. Therefore, the influences of external variables on the sensing performance need to be explored in order to establish a mathematical model, thereby enhancing the adaptability of the SAW gas sensors.

(ii) IDTs play an important role in generating, localizing and transmitting the frequency signals in SAW gas sensors. However, the main challenge is to find a reliable and effective combination of piezoelectric materials and suitable IDT structures to generate efficient wave modes.[220,221] Simulation and modelling have played a valuable role in analyzing and designing the SAW gas sensors.[54] For instance, mathematical and physical methods such as the piezoelectric equation, dispersion equation and wave equation are often used to analyze the propagation characteristics of SAWs in substrates or overlaid structures.[222] Therefore, the period of IDT, the logarithm of IDT, and IDT spacing can be designed through software simulations to improve the quality factor of the SAW device and reduce the insertion loss.

(iii) Porous structured materials have attracted enormous interests in gas sensors due to their highly dispersed active sites at different length scales of pores, which can result in the shortened mass diffusion paths or minimized diffusion barriers, easier accessibility for gas molecules and improved mass transport.[28,63,70,102,131,132,213,223–226] The internal volumes and the concentrations of monomers/additives can be rationally varied to tune the pore size, pore volume, and pore interconnectivity which will in turn affect the mechanical stability, diffusivity, and response sensitivity of the SAW gas sensors.[227,228] Therefore, the porous materials (such as Al_2O_3, SiO_2 and Fe_3O_4) or suitable preparation methods (such as surfactant templating, microporous polymer templating, freeze-drying and sol–gel controlling and post treatment[229]) should be further studied using various modification methods to improve the sensor responses.

(iv) Many strategies for improving the SAW gas sensing performance have been proposed in the literature and briefly discussed in this paper, such as doping and compositing. Doping can change the properties of the morphology and microstructure, electronic structure, and activation energy, and generate oxygen vacancies. For example, oxygen vacancies can serve as the direct adsorption sites as well as electron donor sites and lower activation energy is more beneficial to speed up the rate of the response of the SAW gas sensor. Heterojunctions can be formed at the interfaces of different materials, which can accelerate the transformation of electrons and enhance oxygen adsorption to improve the selectivity and response rates of SAW gas sensors. Therefore, suitable improvement methods should be explored as effective ways to enhance the SAW gas sensing performance.

(v) SAW sensors are developed rapidly for many new fields such as chemical gas detection, military applications and biological detection, and have great potential applications. For example, wearable SAW devices in the military could be used to detect chemical gases used in battlefields, or to monitor soldiers' own biological parameters. Besides, a suitable application is the use of SAW gas sensors in smart food packaging to detect rotten or spoiled food.[230,231] These sensors can accurately identify spoilage gases such as NH_3 in meat and fruit products and can be read by smartphones. Therefore, in the future, intelligent flexible or wearable SAW sensors could be integrated into the daily life of humans to provide more help in their activities.

Conflicts of interest

There are no conflicts to declare.

Acknowledgements

This work was supported by the Key Project of National Natural Science Foundation of China-China Academy of Engineering Physics joint Foundation (NSAF, Grant No. U1830204) and the Engineering Physics and Science Research Council of UK (EPSRC EP/P018998/1) and International Exchange Grant (IEC/NSFC/201078) through the Royal Society and the NSFCC.

References

1 X. Liu, S. Cheng, H. Liu, S. Hu, D. Zhang and H. Ning, *Sensors*, 2012, **12**, 9635–9665.

2 R. Kapoor, S. Ramasamy, A. Gardi, R. V. Schyndel and R. Sabatini, *Sensors*, 2018, **18**, 499.
3 Z. Li, H. Li, Z. Wu, M. Wang, J. Luo, H. Torun, P. A. Hu, C. Yang, M. Grundmann, X. Liu and Y. Q. Fu, *Mater. Horiz.*, 2019, **6**, 470–506.
4 F. J. Kelly and J. C. Fussell, *Environ. Geochem. Health*, 2015, **37**, 631–649.
5 Z. Li, Y. Huang, S. Zhang, W. Chen, Z. Kuang, D. Ao, W. Liu and Y. Fu, *J. Hazard. Mater.*, 2015, **300**, 167–174.
6 Z. S. Hosseini, A. Iraji and A. Mortezaali, *Sens. Actuators, B*, 2015, **207**, 865–871.
7 V. B. Raj, A. T. Nimal, Y. Parmar, M. U. Sharma and V. Gupta, *Sens. Actuators, B*, 2012, **166**, 576–585.
8 N. G. Deshpande, Y. G. Gudage, R. Sharma, J. C. Vyas, J. B. Kim and Y. P. Lee, *Sens. Actuators, B*, 2009, **138**, 76–84.
9 M. Liu, X. Huang, Y. Song, J. Tang, J. Cao, X. Zhang, Q. Zhang, S. Wang, T. Xu, L. Kang, X. Cai, H. Zhang, F. Yang, H. Wang, J. Z. Yu, A. K. H. Lau, L. He, X. Huang, L. Duan, A. Ding, L. Xue, J. Gao, B. Liu and T. Zhu, *Proc. Natl. Acad. Sci.*, 2019, **116**, 7760–7765.
10 K. S. Choi and S. P. Chang, *Mater. Lett.*, 2018, **230**, 48–52.
11 G. Mattoni, B. Jong, N. Manca, M. Tomellini and A. D. Caviglia, *ACS Appl. Nano Mater.*, 2018, **1**, 3446–3452.
12 S. A. Krutovertsev, S. I. Sorokin, A. V. Zorin, Y. A. Letuchy and O. Y. Antonova, *Sens. Actuators, B*, 1992, **7**, 492–494.
13 D. Kwak, Y. Lei and R. Maric, *Talanta*, 2019, **204**, 713–730.
14 C. Caliendo, P. Verardi, E. Verona, A. D. Amico, C. D. Natale, G. Saggio, M. Serafini, R. Paolesse and S. E. Huq, *Smart Mater. Struct.*, 1997, **6**, 689–699.
15 A. Afzal, N. Iqbal, A. Mujahid and R. Schirhagl, *Anal. Chim. Acta*, 2013, **787**, 36–49.
16 T. M. A. Gronewold, *Anal. Chim. Acta*, 2007, **603**, 119–128.
17 W. P. Jakubik, *Thin Solid Films*, 2011, **520**, 986–993.
18 R. M. White and F. W. Voltmer, *Appl. Phys. Lett.*, 1965, **7**, 314.
19 C. C. W. Ruppel, L. Reindl and R. Weigel, *IEEE Microw. Mag.*, 2002, **3**, 65–71.
20 A. Mujahid and F. L. Dickert, *Sensors*, 2017, **17**, 2716.
21 W. Wang, K. Lee, T. Kim, I. Park and S. Yang, *Smart Mater. Struct.*, 2007, **16**, 1382–1389.
22 M. Agostini and M. Cecchini, *Nanotechnology*, 2021, **32**, 312001.
23 L. Lamanna, F. Rizzi, V. R. Bhethanabotla and M. D. Vittorio, *Sens. Actuators, A*, 2020, **315**, 112268.
24 K. Lange, *Sensors*, 2019, **19**, 5382.
25 S. Xiong, J. Zhou, J. Wu, H. Li, W. Zhao, C. He, Y. Liu, Y. Chen, Y. Fu and H. Duan, *ACS Appl. Mater. Interfaces*, 2021, **13**, 42094–42103.
26 J. Devkota, P. R. Ohodnicki and D. W. Greve, *Sensors*, 2017, **17**, 801.
27 E. Chevallier, E. Scorsone and P. Bergonzo, *Sens. Actuators, B*, 2011, **154**, 238–244.
28 H. Zhu, D. Xie, S. Lin, W. Zhang, Y. Yang, R. Zhang, X. Shi, H. Wang, Z. Zhang, X. Zu, Y. Fu and Y. Tang, *Sens. Actuators, B*, 2021, **344**, 130175.
29 J. L. Wang, Y. J. Guo, G. D. Long, Q. B. Tang, X. T. Zu, J. Y. Ma, B. Du, H. Torun and Y. Q. Fu, *J. Hazard. Mater.*, 2020, **388**, 121743.
30 M. Chu, L. Zhou, X. Song, M. Pan, L. Zhang, Y. Sun, J. Zhu and Z. Ding, *Nanotechnology*, 2006, **17**, 1791–1796.
31 A. Mujahid and F. L. Dickert, *Sensors*, 2017, **17**, 2716.
32 Y. Pan, T. Guo, G. Zhang, J. Yang, L. Yang and B. Cao, *Anal. Methods*, 2020, **12**, 2206–2214.
33 W. Wang, H. Hu, X. Liu, S. He, Y. Pan, C. Zhang and C. Dong, *Sensors*, 2016, **16**, 73.
34 V. B. Raj, A. T. Nimal, Y. Parmar, M. U. Sharma and V. Gupta, *Sens. Actuators, B*, 2012, **166**, 576–585.
35 I. Constantinoiu and C. Viespe, *Sensors*, 2020, **20**, 5118.
36 A. Dey, *Mater. Sci. Eng., B*, 2018, **229**, 206–217.
37 T. Zhang, S. Mubeen, N. V. Myung and M. A. Deshusses, *Nanotechnology*, 2008, **19**, 332001.
38 M. Singh, N. Kaur and E. Comini, *J. Mater. Chem. C*, 2020, **8**, 3938–3955.
39 W. Wang, Y. Guo, W. Xiong, Y. Fu, A. Elmarakbi and X. Zu, *Sensors*, 2022, **22**, 6349.
40 W. Wang, S. He, S. Li, M. Liu and Y. Pan, *Sens. Actuators, B*, 2007, **125**, 422–427.
41 O. K. Varghese, P. D. Kichambre, D. Gong, K. G. Ong, E. C. Dickey and C. A. Grimes, *Sens. Actuators, B*, 2001, **81**, 32–41.
42 J. W. Grate, *Chem. Rev.*, 2000, **100**, 2627–2648.
43 H. Yin, Y. Cao, B. Marelli, X. Zeng, A. J. Mason and C. Cao, *Adv. Mater.*, 2021, **33**, 2007764.
44 D. Mandal and S. Banerjee, *Sensors*, 2022, **22**, 820.
45 A. Kumar and R. Prajesh, *Sens. Actuators, A*, 2022, **339**, 113498.
46 B. Wang, L. Sun, M. S. Ramelow, K. D. Lang and H. D. Ngo, *Micromachines*, 2021, **12**, 1429.
47 N. L. L. Hekiem, A. A. M. Ralib, M. A. M. Hattar, F. B. Ahmad, A. N. Nordin and R. A. Rahim, *Sens. Actuators, A*, 2021, **329**, 112792.
48 R. Weser, A. Winkler, M. Weihnacht, S. Menzel and H. Schmidt, *Ultrasonics*, 2020, **106**, 106160.
49 R. M. White and F. W. Voltmer, *Appl. Phys. Lett.*, 1965, **7**, 314.
50 X. Wang, W. Wang, H. Li, C. Fu, K. Ke and S. He, *Sens. Actuators, B*, 2012, **169**, 10–16.
51 S. Thomas, M. Cole, A. D. Luca, F. Torrisi, A. C. Ferrari, F. Udrea and J. W. Gardner, *Procedia Eng.*, 2014, **87**, 999–1002.
52 H. Xu, S. Dong, W. Xuan, U. Farooq, S. Huang, M. Li, T. Wu, H. Jin, X. Wang and J. Luo, *Appl. Phys. Lett.*, 2018, **112**, 093502.
53 T. M. A. Gronewold, *Anal. Chim. Acta*, 2007, **603**, 119–128.
54 Z. Xu and Y. J. Yuan, *Biosens. Bioelectron.*, 2018, **99**, 500–512.
55 K. Länge, *Sensors*, 2019, **19**, 5382.
56 X. Le, Y. Liu, L. Peng, J. Pang, Z. Xu, C. Gao and J. Xie, *Microsyst. Nanoeng.*, 2019, **5**, 36.
57 Y. Liu, Y. Cai, Y. Zhang, A. Tovstopyat, S. Liu and C. Sun, *Micromachines*, 2020, **11**, 630.

58 Y. Jiang, C. Y. Tan, S. Y. Tan, M. S. F. Wong, Y. F. Chen, L. Zhang, K. Yao, S. K. E. Gan, C. Verma and Y. J. Tan, *Sens. Actuators, B*, 2015, **209**, 78–84.
59 G. Martin and B. Wall, *IEEE Trans. Ultrason. Ferroelectrics Freq. Control*, 2000, **47**, 1604–1609.
60 W. Jakubik, J. Wrotniak and P. Powróznik, *Sens. Actuators, B*, 2018, **262**, 947–952.
61 Z. Chen, J. Zhou, H. Tang, Y. Liu, Y. Shen, X. Yin, J. Zheng, H. Zhang, J. Wu, X. Shi, Y. Chen, Y. Fu and H. Duan, *ACS Sens.*, 2020, **5**, 1657–1664.
62 X. Qi, J. Liu, Y. Liang, J. Li and S. He, *Jpn. J. Appl. Phys.*, 2019, **58**, 014001.
63 H. Zhu, D. Xie, S. Lin, W. Zhang, Y. Yang, R. Zhang, X. Shi, H. Wang, Z. Zhang, X. Zu, Y. Fu and Y. Tang, *Sens. Actuators, B*, 2021, **344**, 130175.
64 A. J. Ricco and S. J. Martin, *Thin Solid Films*, 1991, **206**, 94–101.
65 D. Kwak, Y. Lei and R. Maric, *Talanta*, 2019, **204**, 713–730.
66 L. Fan, F. Zhou, C. Wang, H. Gao, S. Zhang, H. Zhang and X. Wang, *IEEE Trans. Ultrason. Ferroelectrics Freq. Control*, 2011, **58**, 451–460.
67 L. Fan, H. Ge, S. Zhang, H. Zhang and J. Zhu, *Sens. Actuators, B*, 2012, **161**, 114–123.
68 L. Fan, Z. Chen, S. Zhang and H. Zhang, *J. Appl. Phys.*, 2014, **115**, 064506.
69 G. Korotcenkov and B. K. Cho, *Sens. Actuators, B*, 2017, **244**, 182–210.
70 M. H. Sun, S. Z. Huang, L. H. Chen, Y. Li, X. Y. Yang, Z. Y. Yuan and B. L. Su, *Chem. Soc. Rev.*, 2016, **45**, 3479–3563.
71 Y. Han, Y. Liu, C. Su, X. Chen, M. Zeng, N. Hu, Y. Su, Z. Zhou, H. Wei and Z. Yang, *Sens. Actuators, B*, 2020, **306**, 127536.
72 G. Chen, X. Chu, H. Qiao, M. Ye, J. Chen, C. Gao and C. Y. Guo, *Mater. Lett.*, 2018, **226**, 59–62.
73 C. Wang, X. Li, C. Feng, Y. Sun and G. Lu, *Sens. Actuators, B*, 2015, **210**, 75–81.
74 Q. Wang, X. Cheng, Y. Wang, Y. Yang, Q. Su, J. Li, B. An, Y. Luo, Z. Wu and E. Xie, *Sens. Actuators, B*, 2022, **355**, 131262.
75 W. Xu, C. Qiu, J. Zhou and Y. Chen, *Ceram. Int.*, 2020, **46**, 11372–11378.
76 Z. Wang, M. Zhi, M. Xu, C. Guo, Z. Man, Z. Zhang, Q. Li, Y. Lv, W. Zhao, J. Yan and C. Zhai, *J. Mater. Sci.*, 2021, **56**, 7348–7356.
77 D. Miu, I. Constantinoiu, C. Enache and C. Viespe, *Nanomaterials*, 2021, **11**, 2598.
78 J. Liu, H. Huang, H. Zhao, X. Yan, S. Wu, Y. Li, M. Wu, L. Chen, X. Yang and B. L. Su, *ACS Appl. Mater. Interfaces*, 2016, **8**, 8583–8590.
79 H. W. Huang, J. Liu, G. He, Y. Peng, M. Wu, W. H. Zheng, L. H. Chen, Y. Li and B. L. Su, *RSC Adv.*, 2015, **5**, 101910.
80 L. Shu, X. Wang, D. Yan, L. Fan and W. Wu, *Materials*, 2019, **12**, 1235.
81 G. Korotcenkov, *Mater. Sci. Eng., B*, 2007, **139**, 1–23.
82 K. Wetchakun, T. Samerjai, N. Tamaekong, C. Liewhiran, C. Siriwong, V. Kruefu, A. Wisitsoraat, A. Tuantranont and S. Phanichphant, *Sens. Actuators, B*, 2011, **160**, 580–591.
83 J. Huang and Q. Wan, *Sensors*, 2009, **9**, 9903–9924.
84 Y. Guo, G. Long, Y. Tang, J. Wang, Q. Tang, X. Zu, J. Ma, B. Du, H. Torun and Y. Fu, *Smart Mater. Struct.*, 2020, **29**, 095003.
85 Z. Liu, T. Fan, D. Zhang, X. Gong and J. Xu, *Sens. Actuators, B*, 2009, **136**, 499–5509.
86 R. Kumar, O. A. Dossary, G. Kumar and A. Umar, *Nano-Micro Lett.*, 2015, **7**, 97–120.
87 Z. Zang and X. Tang, *J. Alloys Compd.*, 2015, **619**, 98–101.
88 A. Saaedi, P. Shabani and R. Yousef, *J. Alloys Compd.*, 2019, **802**, 335–344.
89 J. Dai, O. Ogbeide, N. Macadam, Q. Sun, W. Yu, Y. Li, B. L. Su, T. Hasan, X. Huang and W. Huang, *Chem. Soc. Rev.*, 2020, **49**, 1756–1789.
90 V. B. Raj, H. Singh, A. T. Nimal, M. Tomar, M. U. Sharma and V. Gupta, *Sens. Actuators, B*, 2013, **187**, 563–573.
91 V. B. Raj, H. Singh, A. T. Nimal, M. U. Sharma, M. Tomar and V. Gupta, *Sens. Actuators, B*, 2017, **238**, 83–90.
92 V. B. Raj, A. T. Nimal, Y. P. Parmar, M. U. Sharma, K. Sreenivas and V. Gupta, *Sens. Actuators, B*, 2010, **147**, 517–524.
93 L. Rana, R. Gupta, M. Tomar and V. Gupta, *Sens. Actuators, B*, 2017, **252**, 840–845.
94 A. Marcu and C. Viespe, *Sensors*, 2017, **17**, 1417.
95 A. Marcu and C. Viespe, *Sens. Actuators, B*, 2015, **208**, 1–6.
96 W. Li, Y. Guo, Y. Tang, X. Zu, J. Ma, L. Wang and Y. Q. Fu, *Sensors*, 2017, **17**, 1142.
97 F. C. Huang, Y. Y. Chen and T. T. Wu, *Nanotechnology*, 2009, **20**, 065501.
98 H. Kumar, A. Tripathi, A. B. Dey, M. Gupta, R. Krishna and D. K. Avasthi, *Sens. Actuators, B*, 2019, **301**, 127006.
99 N. Lopez, Z. Łodziana, F. Illas and M. Salmeron, *Phys. Rev. Lett.*, 2004, **93**, 146103.
100 C. Viespe and D. Miu, *Sensors*, 2017, **17**, 1529.
101 T. L. Phan, Y. D. Zhang, D. S. Yang, N. X. Nghia, T. D. Thanh and S. C. Yu, *Appl. Phys. Lett.*, 2013, **102**, 072408.
102 L. Nie, D. Mei, H. Xiong, B. Peng, Z. Ren, X. I. R. Hernandez, A. DeLaRiva, M. Wang, M. H. Engelhard, L. Kovarik, A. K. Datye and Y. Wang, *Science*, 2017, **358**, 1419–1423.
103 A. Ghosh, C. Zhang, S. Shi and H. Zhang, *Sens. Actuators, B*, 2019, **301**, 126958.
104 L. Shu, T. Jiang, Y. Xia, X. Wang, D. Yan and W. Wu, *Sensors*, 2019, **19**, 3025.
105 D. Ao, Z. Li, Y. Fu, Y. Tang, S. Yan and X. Zu, *Nanomaterials*, 2019, **9**, 900.
106 H. Fang, S. Li, H. Zhao, J. Deng, D. Wang and J. Li, *Sens. Actuators, B*, 2022, **352**, 131068.
107 H. Gu, Z. Wang and Y. Hu, *Sensors*, 2012, **12**, 5517–5550.
108 B. P. J. L. Costello, R. J. Ewen, N. M. Ratcliffe and P. S. Sivanand, *Sens. Actuators, B*, 2003, **92**, 159–166.
109 X. Liu, H. Wang, X. Li, D. Liu, J. Wan, X. Lai, S. Hao, Q. Zhang and X. Chen, *Sens. Actuators, B*, 2021, **345**, 130424.
110 L. Chen, S. Bai, G. Zhou, D. Li, A. Chen and C. L. Chung, *Sens. Actuators, B*, 2008, **134**, 360–366.

111 Y. Tang, X. Xu, S. Han, C. Cai, H. Du, H. Zhu, X. Zu and Y. Q. Fu, *Sens. Actuators, B*, 2020, **304**, 127395.
112 Y. L. Tang, Z. J. Li, J. Y. Ma, Y. J. Guo, Y. Q. Fu and X. T. Zu, *Sens. Actuators, B*, 2014, **201**, 114–121.
113 S. Y. Wang, J. Y. Ma, Z. J. Li, H. Q. Su, N. R. Alkurd, W. L. Zhou, L. Wang, B. Du, Y. L. Tang, D. Y. Ao, S. C. Zhang, Q. K. Yu and X. T. Zu, *J. Hazard. Mater.*, 2015, **285**, 368–374.
114 H. Fritzsche, B. Pashmakov and B. Claflin, *Sol. Energy Mater. Sol. Cells*, 1994, **32**, 383–393.
115 S. J. Ippolito, S. Kandasamy, K. Kalantar-zadeh, W. Wlodarski, K. Galatsis, G. Kiriakidis, N. Katsarakis and M. Suchea, *Sens. Actuators, B*, 2005, **111**, 207–212.
116 M. S. Nieuwenhuizen, A. J. Nederlof, M. J. Vellekoop and A. Venema, *Sens. Actuators*, 1989, **19**, 385–392.
117 S. Gong, J. Xia, J. Liu and D. Zhou, *Sens. Actuators, B*, 2008, **134**, 57–61.
118 J. Zhao, S. Wu, J. Liu, H. Liu, S. Gong and D. Zhou, *Sens. Actuators, B*, 2010, **145**, 788–793.
119 W. Luo, Q. Fu, D. Zhou, J. Deng, H. Liu and G. Yan, *Sens. Actuators, B*, 2013, **176**, 746–752.
120 W. Luo, J. Deng, Q. Fu, D. Zhou, Y. Hu, S. Gong and Z. Zheng, *Sens. Actuators, B*, 2015, **217**, 119–128.
121 V. B. Raj, A. T. Nimal, M. Tomar, M. U. Sharma and V. Gupta, *Sens. Actuators, B*, 2015, **220**, 154–161.
122 J. Liu, X. Wang, Q. Peng and Y. Li, *Adv. Mater.*, 2005, **17**, 764–767.
123 L. Yang, C. Yin, Z. Zhang, J. Zhou and H. Xu, *Mater. Sci. Semicond. Process.*, 2017, **60**, 16–28.
124 I. Constantinoiu, D. Miu and C. Viespe, *J. Sens.*, 2019, 2019.
125 X. Wang, W. Wang, H. Li, C. Fu, Y. Ke and S. He, *Sens. Actuators, B*, 2012, **169**, 10–16.
126 M. Penza, G. Cassano and F. Tortorella, *Sens. Actuators, B*, 2001, **81**, 115–121.
127 M. D. Giulio, D. Manno, G. Micocci, A. Serra and A. Tepore, *J. Mater. Sci.: Mater. Electron.*, 1998, **9**, 317–322.
128 K. H. Lee, Y. K. Fang, W. J. Lee, J. J. Ho, K. H. Chen and K. C. Liao, *Sens. Actuators, B*, 2000, **69**, 96–99.
129 C. Wen, C. Zhu, Y. Ju, H. Xu and Y. Qiu, *Sens. Actuators, A*, 2010, **159**, 168–173.
130 T. Kida, A. Nishiyama, M. Yuasa, K. Shimanoe and N. Yamazoe, *Sens. Actuators, B*, 2009, **135**, 568–574.
131 S. J. Ippolito, S. Kandasamy, K. K. Zadeh and W. Wlodarski, *Sens. Actuators, B*, 2005, **108**, 553–557.
132 W. P. Jakubik, *Thin Solid Films*, 2007, **515**, 8345–8350.
133 D. Miu, R. Birjega and C. Viespe, *Sensors*, 2018, **18**, 3636.
134 Y. Zhang, J. Bai, L. Zhou, D. Liu, F. Liu, X. Liang, Y. Gao, F. Liu, X. Yan and G. Lu, *J. Colloid Interface Sci.*, 2019, **536**, 215–223.
135 S. T. Navale, Z. Yang, C. Liu, P. Cao, V. B. Patil, N. S. Ramgir, R. S. Mane and F. J. Stadler, *Sens. Actuators, B*, 2018, **255**, 1701–1710.
136 G. Zhang, H. B. Wu, T. Song, U. Paik and X. W. Lou, *Angew. Chem., Int. Ed.*, 2014, **53**, 12590–12593.
137 H. Liu, W. Li, D. Shen, D. Zhao and G. Wang, *J. Am. Chem. Soc.*, 2015, **137**, 13161–13166.
138 Y. Yu, X. Yin, A. Kvit and X. Wang, *Nano Lett.*, 2014, **14**, 2528–2535.
139 R. Rella, J. Spadavecchia, M. G. Manera, S. Capone, A. Taurino, M. Martino, A. P. Caricato and T. Tunno, *Sens. Actuators, B*, 2007, **127**, 426–431.
140 Y. Tang, D. Ao, W. Li, X. Zu, S. Li and Y. Q. Fu, *Sens. Actuators, B*, 2018, **254**, 1165–1173.
141 I. Constantinoiu and C. Viespe, *Nanomaterials*, 2020, **10**, 760.
142 D. Li, X. Zu, D. Ao, Q. Tang, Y. Q. Fu, Y. Guo, K. Bilawal, M. B. Faheem, L. Li, S. Li and Y. Tang, *Sens. Actuators, B*, 2019, **294**, 55–61.
143 Y. Tang, W. Wu, B. Wang, X. Dai, W. Xie, Y. Yang, R. Zhang, X. Shi, H. Zhu, J. Luo, Y. Guo, X. Xiang, X. Zu and Y. Fu, *Sens. Actuators, B*, 2020, **325**, 128742.
144 G. Kiriakidis, K. Moschovis, I. Kortidis and V. Binas, *Vacuum*, 2012, **86**, 495–506.
145 N. Dewan, S. P. Singh, K. Sreenivas and V. Gupta, *Sens. Actuators, B*, 2007, **124**, 329–335.
146 Y. L. Tang, Z. J. Li, J. Y. Ma, H. Q. Su, Y. J. Guo, L. Wang, B. Du, J. J. Chen, W. Zhou, Q. K. Yu and X. T. Zu, *J. Hazard. Mater.*, 2014, **280**, 127–133.
147 J. Wang, J. Che, C. Qiao, B. Niu, W. Zhang, Y. Han, Y. Fu and Y. Tang, *Sens. Actuators, B*, 2022, **367**, 132160.
148 A. Star, T. R. Han, V. Joshi and J. R. Stetter, *Electroanalysis*, 2004, **16**, 1–2.
149 M. B. Jakubinek, M. A. White, M. Mu and K. I. Winey, *Appl. Phys. Lett.*, 2010, **96**, 083105.
150 O. K. Varghese, P. D. Kichambre, D. Gong, K. G. Ong, E. C. Dickey and C. A. Grimes, *Sens. Actuators, B*, 2001, **81**, 32–41.
151 T. Zhang, M. Mubeen, E. Bekyarova, B. Y. Yoo, R. C. Haddon, N. V. Myung and M. A. Deshusses, *Nanotechnology*, 2007, **18**, 165504.
152 S. Sivaramakrishnan, R. Rajamani, C. S. Smith, K. A. McGee, K. R. Mann and N. Yamashita, *Sens. Actuators, B*, 2008, **132**, 296–304.
153 L. Zhang, D. M. Sun, P. X. Hou, C. Liu, T. Liu, J. Wen, N. Tang, J. Luan, C. Shi, J. C. Li, H. T. Cong and H. M. Cheng, *Adv. Mater.*, 2017, **29**, 1605719.
154 S. Jiang, P. X. Hou, M. L. Chen, B. W. Wang, D. M. Sun, D. M. Tang, Q. Jin, Q. X. Guo, D. D. Zhang, J. H. Du, K. P. Tai, J. Tan, E. I. Kauppinen, C. Liu and H. M. Cheng, *Sci. Adv.*, 2018, **4**, eaap9264.
155 E. H. Espinosa, R. Ionescu, C. Bittencourt, A. Felten, R. Erni, G. V. Tendeloo, J.-J. Pireaux and E. Llobet, *Thin Solid Films*, 2007, **515**, 8322–8327.
156 M. K. Kumar and S. Ramaprabhu, *J. Phys. Chem. B*, 2006, **110**, 11291–11298.
157 M. Penza, F. Antolini and M. V. Antisari, *Sens. Actuators, B*, 2004, **100**, 47–59.
158 M. Penza, P. Aversa, G. Cassano, W. Wlodarski and K. K. Zadeh, *Sens. Actuators, B*, 2007, **127**, 168–178.
159 S. Kim, H. R. Lee, Y. J. Yun, S. Ji, K. Yoo, W. S. Yun, J. Y. Koo and D. H. Ha, *Appl. Phys. Lett.*, 2007, **91**, 093126.
160 J. Y. Jeon, B. C. Kang and T. J. Ha, *Appl. Surf. Sci.*, 2020, **514**, 145956.

161 X. Feng, S. Irle, H. Witek, K. Morokuma, R. Vidic and E. Borguet, *J. Am. Chem. Soc.*, 2005, **127**, 10533–10538.
162 J. Kong, M. G. Chapline and H. Dai, *Adv. Mater.*, 2001, **13**, 1384–1386.
163 S. Tang, W. Chen, H. Zhang, Z. Song, Y. Li and Y. Wang, *Front. Chem.*, 2020, **8**, 174.
164 M. Asad and M. H. Sheikhi, *Sens. Actuators, B*, 2014, **198**, 134–141.
165 N. Zhang, K. Yu, Q. Li, Z. Q. Zhu and Q. Wan, *J. Appl. Phys.*, 2008, **103**, 104305.
166 S. Zhu, X. Liu, Z. Chen, C. Liu, C. Feng, J. Gu, Q. Liu and D. Zhang, *J. Mater. Chem.*, 2010, **20**, 9126–9132.
167 J. Duan, J. Xiang, X. Sun, C. Xu, S. Wang and Y. Hu, *IEEE Sens. J.*, 2016, **16**, 287–292.
168 Z. Yunusa, M. N. Hamidon, A. Ismail, M. M. Isa, M. H. Yaacob, S. Rahmanian, S. A. Ibrahim and A. A. A. Shabaneh, *Sensors*, 2015, **15**, 4749–4765.
169 I. Sayago, M. J. Fernández, J. L. Fontecha, M. C. Horrillo, C. Vera, I. Obieta and I. Bustero, *Sens. Actuators, B*, 2012, **175**, 67–72.
170 D. Pandey, R. Reifenberger and R. Piner, *Surf. Sci.*, 2008, **602**, 1607–1613.
171 D. R. Dreyer, S. Park, C. W. Bielawski and R. S. Ruoff, *Chem. Soc. Rev.*, 2010, **39**, 228–240.
172 S. Eigler, C. Dotzer, F. Hof, W. Bauer and A. Hirsch, *Chem. - Eur. J.*, 2013, **19**, 9490–9496.
173 I. Sayago, D. Matatagui, M. J. Fernández, J. L. Fontecha, I. Jurewicz, R. Garriga and E. Muñoz, *Talanta*, 2016, **148**, 393–400.
174 Q. Tang, Y. Guo, Y. Tang, G. Long, J. Wang, D. Li, X. Zu, J. Ma, L. Wang, H. Torun and Y. Fu, *J. Mater. Sci.*, 2019, **54**, 11925–11935.
175 D. Li, X. Le, J. Pang, L. Peng, Z. Xu, C. Gao and J. Xie, *J. Micromech. Microeng.*, 2019, **29**, 045007.
176 R. Arsat, M. Breedon, M. Shafiei, P. G. Spizziri, S. Gilje, R. B. Kaner, K. K. Zadeh and W. Wlodarski, *Chem. Phys. Lett.*, 2009, **467**, 344–347.
177 B. S. Joo, J. S. Huh and D. D. Lee, *Sens. Actuators, B*, 2007, **121**, 47–53.
178 Y. Yan, G. Yang, J. L. Xu, M. Zhang, K. K. Kuo and S. D. Wang, *Sci. Technol. Adv. Mater.*, 2020, **21**, 768–786.
179 J. W. Grate, *Chem. Rev.*, 2000, **100**, 2627–2648.
180 E. T. Zellets, S. A. Batterman, M. Han and S. J. Patrash, *Anal. Chem.*, 1995, **67**, 1092–1106.
181 J. W. Grate, *Chem. Rev.*, 2008, **108**, 726–745.
182 D. Amati, D. Arn, N. Blom, M. Ehrat, J. Saunois and H. M. Widmer, *Sens. Actuators, B*, 1992, **7**, 587–591.
183 D. Rabus, J. M. Friedt, L. Arapan, S. Lamare, M. Baqué, G. Audouin and F. Chérioux, *ACS Sens.*, 2020, **5**, 1075–1081.
184 C. Y. Shen and S. Y. Liou, *Sens. Actuators, B*, 2008, **131**, 673–679.
185 S. Virji, J. Huang, R. B. Kaner and B. H. Weiller, *Nano Lett.*, 2004, **4**, 491–496.
186 S. Virji, J. D. Fowler, C. O. Baker, J. Huang, R. B. Kaner and B. H. Weiller, *Small*, 2005, **1**, 624–627.
187 A. Z. Sadek, C. O. Baker, D. A. Powell, W. Wlodarski, R. B. Kaner and K. K. Zadeh, *IEEE Sens. J.*, 2007, **7**, 213–218.
188 A. Z. Sadek, W. Wlodarski, K. Kalantar-zadeh, K. Shin and B. Kaner, *Sensors*, 2006, **2006**, 687–690.
189 X. Liu, W. Wang, Y. Zhang, Y. Pan, Y. Liang and J. Li, *Sensors*, 2018, **18**, 3796.
190 S. Qin, Z. Wu, Z. Tang, Y. Song, F. Zeng and D. Zhao, *Sens. Actuators, B*, 2000, **66**, 240–242.
191 S. Liu, H. Sun, R. Nagarajan, J. Kumar, Z. Gu, J. Cho and P. Kurup, *Sens. Actuators, A*, 2011, **167**, 8–13.
192 B. Lakard, O. Segut, S. Lakard, G. Herlem and T. Gharbi, *Sens. Actuators, B*, 2007, **122**, 101–108.
193 L. A. Mashat, H. D. Tran, W. Wlodarski, R. B. Kaner and K. K. Zadeh, *Sens. Actuators, B*, 2008, **134**, 826–831.
194 X. Chen, D. M. Li, S. F. Liang, S. Zhan and M. Liu, *Sens. Actuators, B*, 2013, **177**, 364–369.
195 K. S. Pasupuleti, N. H. Bak, K. R. Peta, S. G. Kim, H. D. Cho and M. D. Kim, *Sens. Actuators, B*, 2022, **363**, 131786.
196 T. Chobsilp, T. Threrujirapapong, V. Yordsri, A. Treetong, S. Inpaeng, K. Tedsree, P. Ayala, T. Pichler, L. Shi and W. Muangrat, *Sensors*, 2022, **22**, 9329.
197 A. Mirmohseni and A. Oladegaragoze, *Sens. Actuators, B*, 2003, **89**, 164–172.
198 X. He, R. Arsat, A. Z. Sadek, W. Wlodarski, K. K. Zadeh and J. Li, *Sens. Actuators, B*, 2010, **145**, 674–679.
199 D. Matatagui, M. J. Fernandez, J. P. Santos, J. Fontecha, I. Sayago, M. C. Horrillo, I. Gracia and C. Cane, *J. Nanomater.*, 2014, 243037.
200 M. Teodorescu and M. Bercea, *Polym.-Plast. Technol. Eng.*, 2015, **9**, 923–943.
201 P. S. Chee, R. Arsat, X. He, K. K. Zadeh, M. Arsat and W. Wlodarski, *AIP Conf. Proc.*, 2011, **1341**, 410–414.
202 S. Liu, H. Sun, R. Nagarajan, J. Kumar, Z. Gu, J. H. Cho and P. Kurup, *Sens. Actuators, A*, 2011, **167**, 8–13.
203 Y. Tang, X. Xu, H. Du, H. Zhu, D. Li, D. Ao, Y. Guo, Y. Q. Fu and X. Zu, *Sens. Actuators, A*, 2020, **301**, 111792.
204 J. Wang, Y. Guo, G. Long, Y. Tong, Q. Tang, X. Zu, J. Ma, B. Du, H. Torun and Y. Fu, *J. Hazard. Mater.*, 2020, **388**, 121743.
205 Y. Tang, D. Li, D. Ao, Y. Guo, M. B. Faheem, B. Khan, X. Zu and S. Li, *Mater. Chem. Phys.*, 2020, **239**, 122026.
206 D. Sil, J. Hines, U. Udeoyo and E. Borguet, *ACS Appl. Mater. Interfaces*, 2015, **7**, 5709–5714.
207 A. D. Amico, A. Palma and E. Verona, *Appl. Phys. Lett.*, 1982, 41.
208 C. Viespe, V. Dinca, G. P. Pelin and D. Miu, *Sensors*, 2019, **19**, 4492.
209 Z. Li, W. Yang, M. Huang, X. Yang, C. Zhu, C. He, L. Li, Y. Wang, Y. Xie, Z. Luo, D. Liang, J. Huang, X. Zhu, X. Zhuang, D. Li and A. Pan, *Opto-Electron. Adv.*, 2021, **4**, 210017.
210 Z. Zheng, X. Zu, Y. Zhang and W. Zhou, *Mater. Today Phys.*, 2020, **15**, 100262.
211 G. Long, Y. Guo, W. Li, Q. Tang, X. Zu, J. Ma, B. Du and Y. Fu, *Microelectron. Eng.*, 2020, **222**, 111201.
212 M. Li, H. Kan, S. Chen, X. Feng, H. Li, C. Li, C. Fu, A. Quan, H. Sun, J. Luo, X. Liu, W. Wang, H. Liu, Q. Wei and Y. Q. Fu, *Sens. Actuators, B*, 2019, **287**, 241–249.

213 H. Li, M. Li, H. Kan, C. Li, A. Quan, C. Fu, J. Luo, X. Liu, W. Wang, Z. Yang, Q. Wei and Y. Fu, *Surf. Coat. Technol.*, 2019, **362**, 78–83.
214 G. Konstantatos, L. Levina, J. Tang and E. H. Sargent, *Nano Lett.*, 2008, **8**, 4002–4006.
215 G. Li, X. Chen and G. Gao, *Nanoscale*, 2014, **6**, 3283–3288.
216 Z. Zhang, M. Morgan, P. Maji, X. Xiang, X. Zu and W. Zhou, *RSC Adv.*, 2023, **13**, 3487–3493.
217 J. Luo, X. Feng, H. Kan, H. Li and C. Fu, *IEEE Sens. J.*, 2021, **21**, 1404–1408.
218 J. Pang, X. Le, K. Pang, H. Dong, Q. Zhang, Z. Xu, C. Gao, Y. Fu and J. Xie, *Sens. Actuators, B*, 2021, **338**, 129824.
219 J. Wei, C. Yin, J. Zhou, H. Li, Y. Liu, Y. Shen, S. Garner, Y. Fu and H. Duan, *ACS Appl. Mater. Interfaces*, 2020, **12**, 39817–39825.
220 D. Fall, M. Duquennoy, M. Ouaftouh, B. Piwakowski and F. Jenot, *Ultrasonics*, 2018, **82**, 371–378.
221 T. Aubert, O. Elmazria, B. Assouar, L. Bouvot, M. Hehn, S. Weber, M. Oudich and D. Genève, *IEEE Trans. Ultrason. Ferroelectrics Freq. Control*, 2011, **58**, 603–610.
222 D. A. Powell, K. K. Zadeh and W. Wlodarski, *Sens. Actuators, A*, 2004, **115**, 456–461.
223 M. Z. Atashbar, A. Z. Sadek, W. Wlodarski, S. Sriram, M. Bhaskaran, C. J. Cheng, R. B. Kaner and K. Kalantar-zadeh, *Sens. Actuators, B*, 2009, **138**, 85–89.
224 G. Korotcenkov, *Nanomaterials*, 2021, **11**, 1555.
225 O. Ogbeide, G. Bae, W. Yu, E. Morrin, Y. Song, W. Song, Y. Li, B. L. Sun, K. S. An and T. Hasan, *Adv. Funct. Mater.*, 2022, **32**, 2113348.
226 T. C. Wu, J. Dai, G. Hu, W. B. Yu, O. Ogbeide, A. D. Luca, X. Huang, B. L. Su, Y. Li, F. Udrea and T. Hasan, *Sens. Actuators, B*, 2020, **321**, 128446.
227 M. A. Mudassir, H. Z. Aslam, T. M. Ansari, H. Zhang and I. Hussain, *Adv. Sci.*, 2021, **8**, 2102540.
228 J. Dai, O. Ogbeide, N. Macadam, Q. Sun, W. Yu, Y. Li, B. L. Su, T. Hasan, X. Huang and W. Huang, *Chem. Soc. Rev.*, 2020, **49**, 1756–1789.
229 X. Y. Yang, L. H. Chen, Y. Li, J. C. Rooke, C. Sanchez and B. L. Su, *Chem. Soc. Rev.*, 2017, **46**, 481–558.
230 M. V. Nikolic, V. Milovanovic, Z. Z. Vasiljevic and Z. Stamenkovic, *Sensors*, 2020, **20**, 6694.
231 Q. Feng, X. Zu, B. Wang, L. Sun, B. Li, X. Xiang, L. Li, Y. Tian, X. Yuan, W. Zheng, H. Yang, H. Deng, S. Li and H. Deng, *J. Mater. Res. Technol.*, 2022, **21**, 2906–2914.

